Biogeosciences Discuss., doi:10.5194/bg-2016-308, 2016
Manuscript under review for journal Biogeosciences
Published: 9 August 2016

Biogeosciences Discussions
Open Access
EGU

Low methane concentrations in sediment along the continental slope north of Siberia: Inference from pore water geochemistry

Clint M. Miller[1], Gerald R. Dickens[1], Martin Jakobsson[2], Carina Johansson[2], Andrey Koshurnikov[3], Matt O'Regan[2], Francesco Muschitiello[2], Christian Stranne[2], Carl-Magnus Mörth[2]

A manuscript submitted to:

Biogeosciences

[July 23, 2016]

[1]Department of Earth Science, Rice University, Houston, TX, USA

[2]Department of Geological Sciences, Stockholm University, Stockholm, Sweden

[3]V.I. Il'ichev Pacific Oceanological Institute, RAS

Biogeosciences Discuss., doi:10.5194/bg-2016-308, 2016
Manuscript under review for journal Biogeosciences
Published: 9 August 2016

Abstract: The Eastern Siberian Margin (ESM), a vast region of the Arctic, potentially holds large amounts of methane in sediments as gas hydrate and free gas. Although this CH_4 has become a topic of discussion, primarily because of rapid regional climate change, the ESM remains sparingly explored. Here we present pore water chemistry results from 32 cores taken during Leg 2 of the 2014 SWERUS-C3 expedition. The cores come from depth transects across the continental slope of the ESM between Wrangel Island and the New Siberian Islands. Upward CH_4 flux towards the seafloor, as inferred from profiles of dissolved sulfate (SO_4^{2-}), alkalinity, and the δ^{13}C-dissolved inorganic Carbon (DIC), is negligible at all stations east of where the Lomonosov Ridge abuts the ESM at about 143°E. In the upper eight meters of these cores, downward sulfate flux never exceeds 9.2 mol/m^2-kyr, the upward alkalinity flux never exceeds 6.8 mol/m^2-kyr, and δ^{13}C-DIC only slowly decreases with depth (-3.6‰/m on average). Additionally, dissolved H_2S was not detected in these cores, and nutrient and metal profiles reveal that metal oxide reduction by organic carbon dominates the geochemical environment. A single core on Lomonosov Ridge differs, as diffusive fluxes for SO_4^{2-} and alkalinity were 13.9 and 11.3 mol/m^2-kyr, respectively, the δ^{13}C-DIC gradient was 5.6‰/m, and Mn^{2+} reduction terminated within 1.3 m of the seafloor. These are among the first pore water results generated from this vast climatically sensitive region, and they imply that significant quantities of CH_4, including gas hydrates, do not exist in any of our investigated depth transects spread out along much of the ESM continental slope. This contradicts previous assumptions and hypothetical models and discussion, which generally have assumed the presence of substantial CH_4.

Biogeosciences Discuss., doi:10.5194/bg-2016-308, 2016
Manuscript under review for journal Biogeosciences
Published: 9 August 2016

1. Introduction

The Arctic is especially sensitive to global climate change. Already, over the last century, the region has experienced some of the fastest rates of warming on Earth (Serreze et al., 2000; Peterson et al., 2002; Semiletov et al., 2004). Past and future increases in atmospheric and surface water temperatures should, with time, lead to substantial warming of intermediate to deep waters (Dmitrenko et al., 2008; Spielhagen et al., 2011), as well as sediment beneath the seafloor (Reagan and Moridis, 2009; Phrampus et al., 2014). The latter is both fascinating and worrisome, because pore space within the upper few hundreds of meters of sediment along many continental slopes can contain large amounts of temperature-sensitive methane (CH_4) in gas hydrates, free gas, and dissolved gas (Kvenvolden, 1993 and 2001; Beaudoin et al., 2014). Consequently, numerous papers have discussed the potential impact of future warming upon CH_4 within slopes of the Arctic Ocean (Paull et al., 1991; Archer, 2007; Reagan and Moridis, 2008; McGuire et al., 2009; Biastoch et al., 2011; Elliott et al., 2011; Ferré et al., 2012; Giustiniani et al., 2013; Thatcher et al., 2013; Stranne et al., 2016).

Globally, the distribution and total amount of CH_4 in sediment along continental slopes remains poorly constrained (Beaudoin et al., 2014). This is particularly true for the Arctic Ocean, because ice cover makes accessibility to many regions difficult. Nonetheless, numerous papers have inferred enormous quantities of gas hydrate surrounding the Arctic (Kvenvolden and Grantz, 1990; Max and Lowrie, 1993; Buffett and Archer, 2004; Klauda and Sandler, 2005; Max and Johnson, 2012; Wallmann et al., 2012; Piñero et al., 2013; **Figure 1**). In some sectors, compelling evidence exists for abundant sedimentary CH_4 and gas hydrate. Bottom simulating reflectors (BSRs) on seismic profiles generally mark the transition between overlying gas hydrate and underlying free gas (Holbrook et al., 1996; Pecher et al., 2001), and thereby imply

Biogeosciences Discuss., doi:10.5194/bg-2016-308, 2016
Manuscript under review for journal Biogeosciences
Published: 9 August 2016

high quantities of CH_4 in pore space (Dickens et al., 1997; Pecher et al., 2001). Such BSRs have been documented along the North Slope of Alaska (Collett, 2002; Collett et al., 2010), within the Beaufort Sea (Grantz et al., 1976; Grantz et al., 1982; Weaver and Stewart, 1982; Hart et al., 2011; Phrampus et al., 2014), around Canadian Arctic Islands (Judge, 1982; Hyndman and Dallimore, 2001; Majorowicz and Osadetz, 2001; Yamamoto and Dallimore, 2008), adjacent to Svalbard (Eiken and Hinz, 1993; Posewang and Mienert, 1999; Vanneste et al., 2005; Hustoft et al., 2009; Petersen et al., 2010), and within the Barents Sea (Andreassen et al. 1990; Løvø et al., 1990; Laberg and Andreassen, 1996; Laberg et al., 1998; Chand et al., 2008; Ostanin et al., 2013). Furthermore, Lorenson and Kvenvolden (1995) observed high CH_4 concentrations in shelf waters of the Beaufort Sea and Shakhova (2010a, 2010b) have documented ample evidence for methane escape to the water column on the East Siberian Margin (ESM). It generally has been assumed that sediment on the adjacent ESM slope contains copious CH_4 and gas hydrate (**Figure 1**), although no scientific expedition has investigated the hypothesis.

Regional assessments for the presence of abundant CH_4 in marine sediment can be acquired through two general approaches. The first includes geophysical applications, primarily seismic reflection profiling and the recognition of BSRs (MacKay et al., 1994; Carcione and Tinivella, 2000; Haacke et al., 2008), which are a common, but not ubiquitous feature, of hydrate bearing sediments. The second utilizes chemical analyses of pore waters obtained from short sediment cores (Borowski et el., 1996; Borowski et al., 1999; Kastner et al., 2008b; Dickens and Snyder 2009). In marine sediments with abundant CH_4, a general and important process occurs near the seafloor, typically within the upper 30 m. Upward migrating methane, either through advection or diffusion, reacts with downward diffusing sulfate (SO_4^{2-}):

$$^{12}CH_4 + SO_4^{2-} \rightarrow HS^- + H^{12}CO_3^- + H_2O \quad (1)$$

Biogeosciences Discuss., doi:10.5194/bg-2016-308, 2016
Manuscript under review for journal Biogeosciences
Published: 9 August 2016

where the superscript ^{12}C denotes that methane is depleted in ^{13}C. This microbially mediated reaction (Barnes and Goldberg, 1976; Reeburgh, 1976; Devol and Ahmed, 1981; Boetius et al., 2000), commonly called anaerobic oxidation of methane (AOM), leads to characteristic pore water chemistry profiles, including a clearly recognizable sulfate methane transition (SMT; **Figure 2**). The depth of the SMT inversely relates to the flux of CH_4 (Dickens, 2001; Bhatnagar, 2011). Where CH_4 to the seafloor is high, the SMT is located at shallow depth. Along the continental shelf and slope of the Beaufort Sea, where seismic profiles indicate gas hydrate, Coffin et al. (2008, 2013) predictably have documented SMTs in shallow sediment.

The joint Swedish, Russian, U.S. Arctic Ocean Investigation of Climate-Cryosphere-Carbon interaction (SWERUS-C3) project was initiated to investigate spatial changes in carbon cycling across the ESM. A central theme of this project was to constrain the amount, distribution, and fluxes of CH_4, and included a two-leg expedition in the boreal summer of 2014 using the Swedish icebreaker *IB Oden*. Efforts of Leg 2 (8/21-10/3) included retrieval of 60 piston/gravity/multi cores of which six piston, seven gravity, and 17 multicores spanning the continental slope of the ESM are studied here (**Figure 3**). A total of 446 pore water samples were collected from these cores to document changes in chemistry associated with expected SMTs. Here we present and discuss analytical results of these samples. Surprisingly, pore water profiles strongly indicate that, contrary to general inferences, very little CH_4 exists in shallow sediment along the continental slope north of Siberia, which may preclude the presence of gas hydrate.

2. Background

2.1 East Siberian Margin Geology

Biogeosciences Discuss., doi:10.5194/bg-2016-308, 2016
Manuscript under review for journal Biogeosciences
Published: 9 August 2016

104 Extensive continental shelves and their associated slopes nearly enclose the central Arctic
105 Ocean (**Figure 1**). Although it represents only 2.6% of the world's ocean by area (Jakobsson,
106 2002), the central Arctic Ocean receives approximately 10% of the global freshwater input
107 (Stein, 2008) as well as corresponding massive discharge of terrigenous material (>249 Mt/yr;
108 Holmes et al., 2002). Only Fram Strait allows deep-water flow to and from the Arctic Ocean.
109 This strait, located between Greenland and Svalbard (**Figure 1**), has today a sill depth of about
110 2540 m (Jakobsson et al., 2003). It opened from early to middle Miocene times (Jakobsson et al.,
111 2007; Engen et al., 2008; Hustoft et al., 2009). Prior to this, the central Arctic Ocean only
112 connect to the world oceans through shallow seaways (e.g., Turgay Straight), and deep waters
113 may have been anoxic for long intervals of the Cretaceous and Paleogene (Clark, 1988; O'Regan
114 et al., 2011). Sediments with very high total organic carbon (TOC) accumulated on Lomonosov
115 Ridge during the middle Eocene (Stein et al., 2006), and on Alpha Ridge during the late
116 Cretaceous (Jenkyns et al., 2004).
117 The ESM is here defined to comprise the margin of the East Siberian Sea, which stretches
118 between Wrangel Island to the east and the New Siberian Islands to the west (**Figure 3**). We
119 include the adjacent continental slope in the ESM. This stretch of continental shelf is the widest
120 in the world, extending 1500 km north from the coast. The huge swath laying in water depths
121 less than 100 m (~987 x 10^3 km^2; Jakobsson, 2002) was for the most part, aerially exposed
122 during glacial periods, resulting in extensive formation of submarine permafrost (Judge, 1982;
123 Weaver and Stewart, 1982; Løvø et al., 1990; Collett et al., 2010). The expansive shelf contrasts
124 with the relative narrow continental slope, which intersects two ridge systems, Mendeleev Ridge
125 to the east and Lomonosov Ridge to the west (Jakobsson et al., 2008). Bounded by these two

Biogeosciences Discuss., doi:10.5194/bg-2016-308, 2016
Manuscript under review for journal Biogeosciences
Published: 9 August 2016

126 ridge systems, the steep ESM slope leads into the gently sloping Chukchi, Arlis, and Wrangel
127 perched continental rises (Jakobsson et al., 2003).
128
129 *2.2 Regional Oceanography*
130 Bottom waters impinging the slope of the ESM can generally be divided into three masses:
131 the Pacific Halocline (~50-200m), the Atlantic Layer (~200-800m), and Canada Basin Bottom
132 Water (>800m; Timokhov, 1994; Rudels et al., 2000). The Pacific Halocline is a cold (-1.5-0°C),
133 low salinity (32-33.5 psu) water mass that serves as a boundary (and heat sink) between sea ice
134 (above) and Atlantic Layer water (below) (Aagaard, 1981; Aagaard and Carmack, 1989). The
135 underlying Atlantic Layer is warmer (>0°C) but more saline (33.5-34.5 psu; Rudels et al., 2000).
136 The Atlantic Layer water originates from water arriving to the ESM region partly through Fram
137 Strait via the West Spitsbergen Current and partly over the Barents Sea through St. Anna
138 Trough. The inflow from the Atlantic has been observed to vary over time, specifically striking
139 are observations of warm pulses influencing the core temperature of the Atlantic Layer in the
140 central Arctic Ocean on decadal time scales (Dmitrenko et al., 2009; Woodgate et al., 2001).
141 Canada Basin Bottom Water is colder (~-0.5°C) and relatively saline (~34.9 psu), with a
142 residence time exceeding 300 years (Stein, 2008). The upper halocline shields the lower warmer
143 waters, which may promote sea ice formation (Aagaard and Carmack, 1989). The aspect
144 motivating our study is that climate warming could increase bottom water temperatures on the
145 shelf slope, in the sensitive feather edge of hydrate stability (300-450 m, Stranne et al., 2016),
146 which would decrease the extent of the gas hydrate stability zone (GHSZ) and possibly release
147 CH_4 to the water column and atmosphere.
148

Biogeosciences Discuss., doi:10.5194/bg-2016-308, 2016
Manuscript under review for journal Biogeosciences
Published: 9 August 2016

149 *2.3 Current Speculation on Gas Hydrates in the Arctic*

150 Even during summer months over the last decade, 2-3 m of sea ice covers much of the
151 Arctic Ocean adjacent to Siberia (Stroeve et al., 2012). This necessitates the use of large ice
152 breaking vessels to explore the region. Consequently, limited information exists regarding
153 continental slopes of the ESM. Four icebreaker expeditions, the 1995 Polarstern Expedition
154 ARK-XI/1 [Rachor, 1995], the 1996 Arctic Ocean Expedition ARK-XII/1 [Augstein et al.,
155 1997], the 2008 Polarstern Expedition ARK-XXIII/3 [Jokat, 2010], and the 2009 Russian-
156 American RUSALCA Expedition [Bakhmutov et al., 2009] have retrieved geophysical data and
157 sediment on or adjacent to the ESM slope.

158 So far, no drilling has occurred on the ESM slope. However, the 2004 Arctic Coring
159 Expedition (ACEX; Backman et al., 2009) drilled and cored the central Lomonosov Ridge
160 (**Figure 1**). There are also land based studies (Gualtier et al., 2005; Sher et al., 2005; Andreev et
161 al., 2009), and some public Oil and Gas Exploration materials which provide indirect data on the
162 ESM (Hovland and Svensen, 2006).

163 Despite the paucity of ground-truth data, as shown by maps of conjectured Arctic gas
164 hydrate distribution (**Figure 1**), many researchers have predicted widespread and abundant CH_4,
165 including gas hydrate, along the ESM continental slope. This is a logical inference that arose for
166 two main reasons. First, particulate organic carbon (POC) provides the ultimate source of CH_4 in
167 marine sediments (Kvenvolden and Grantz, 1990), and Arctic slopes may contain high POC
168 contents, which accumulated prior to the opening of the Fram Strait (Jokat and Ickrath, 2015), or
169 along with terrigenous material during interglacial intervals of the Quaternary (Danyushevskaya
170 et al., 1980; Clark, 1988; Darby, 1989; Moran et al., 2006; Archer, 2015). Certainly, organic rich
171 Eocene sediments have been documented on other Arctic margins and in the ACEX cores on

Biogeosciences Discuss., doi:10.5194/bg-2016-308, 2016
Manuscript under review for journal Biogeosciences
Published: 9 August 2016

Lomonosov Ridge (Moran et al., 2006; Backman and Moran, 2009; O'Regan et al., 2011). Moreover, during Pleistocene glacial periods, extensive portions of the adjacent continental shelf were subaerially exposed tundra (Gusev et al., 2009; Jakobsson et al., 2014), and the locus of sediment deposition moved toward the slope (Alekseev, 1997; Naidu et al., 2000; Niessen et al., 2013). Organic matter burial might be enhanced further by cold seafloor temperatures, which should reduce bacterial degradation in shallow sediment (Darby et al., 1989; Max and Lowrie, 1993). Second, the thickness of the GHSZ depends on bottom water temperature and the geothermal gradient (Dickens, 2001), and very low bottom water temperatures along the slope combined with low geothermal gradients (O'Regan et al., 2016) imply a volumetrically extensive GHSZ (Miles, 1995; Makogon, 2010). Few environmental considerations point against the existence of gas hydrates in the ESM slopes although glacial periods dominated by relatively low sea levels might have kept the sensitive shallow part of the present GHSZ depleted of hydrates (Stranne et al., 2016).

2.4 Pore Water Chemistry Above Methane-Charged Sediment Sequences

Pore water chemistry profiles provide a powerful means to constrain CH_4 abundance and fluxes in marine sediment sequences (Borowski et al., 1996; Berg et al., 1998; Jørgensen et al., 2001; Torres and Kastner, 2009; Treude et al., 2014). Such profiles are generated by extracting interstitial water from sediment cores, and measuring the concentrations of dissolved species. In the absence of significant advection, depth profiles of various analytes relate to Fick's law of diffusion and chemical reactions (e.g., Berner, 1977; Froelich et al., 1979; Klump and Martens 1981; Schulz, 2000).

Biogeosciences Discuss., doi:10.5194/bg-2016-308, 2016
Manuscript under review for journal Biogeosciences
Published: 9 August 2016

194 The flux (J) of a dissolved species through porous marine sediment can be calculated from
195 the concentration gradient by (Li & Gregory, 1974; Berner, 1975; Lerman, 1977):

196 $$J = -\varphi D_s \frac{\partial C}{\partial Z}, \quad (2)$$

197 where φ is porosity, D_s is the diffusivity of an ion in sediment at a specified temperature, C is
198 concentration, and Z is depth. Note that, as generally written, J is positive for upward fluxes and
199 negative for downward fluxes relative to the seafloor. In many locations, φ and D_s change only
200 moderately (<20%) in the upper few tens of meters below the seafloor. However, abundant CH_4
201 in sediment necessarily leads to a large concentration gradient toward the seafloor and a major
202 upward flux of CH_4. The consequent reaction with SO_4^{2-} via AOM (**Equation 1**) leads to a series
203 of flux changes in dissolved components (addition or removal), and predictable variations in
204 corresponding concentration profiles across a SMT (Alperin, 1988; Niewohner et al., 1998;
205 Ussler and Paull, 2008; Dickens and Snyder, 2009; Regnier et al., 2011).
206 Typically, the SMT is a thin (<2 m) depth horizon with major inflections in both CH_4 and
207 SO_4^{2-} profiles (**Figure 2**). Sulfate concentrations decrease from seawater values at the seafloor to
208 zero at the SMT; by contrast, CH_4 concentrations rise from zero at the SMT to elevated values at
209 depth. In regions dominated by diffusion, the depth of the SMT relates to the flux of CH_4 from
210 below (Jørgensen et al., 1990; Dickens, 2001; D'Hondt et al., 2002; Hensen et al., 2003). In part,
211 this is because SO_4^{2-} concentrations at the seafloor are fixed.
212 Importantly, as one can infer from **Equations 1 and 2**, AOM affects additional species
213 dissolved in pore water (Alperin et al., 1988; Jørgensen et al., 1990; Dickens, 2001; Hensen et
214 al., 2003; Snyder et al., 2007). Dissolved HS^- and HCO_3^- concentrations necessarily increase
215 across the SMT, so an inflection occurs in their concentration profiles. These two species

Biogeosciences Discuss., doi:10.5194/bg-2016-308, 2016
Manuscript under review for journal Biogeosciences
Published: 9 August 2016

contribute to total alkalinity (Gieskes and Rogers, 1973; Haraldsson et al., 1997), which can be defined as:

$$Alk_T = [HCO_3^-] + 2[CO_3^{2-}] + [HS^-] + [B(OH)_4^-] + [OH^-] + [HPO_4^{2-}] + [NH_3] + [X]\,, \quad (3)$$

over the pH range 6.3 to 10.3, where X refers to several minor species. However, in shallow sediments found above almost all CH_4 charged systems, this can be expressed as:

$$Alk_T \approx [HCO_3^-] + [HS^-]\,, \quad (4)$$

Thus, with the production of HS^- and HCO_3^-, an inflection in Alk_T occurs across the SMT (Luff and Wallmann 2003; Dickens and Snyder, 2009; Jørgensen and Parkes, 2010; Smith and Coffin, 2014; Ye et al., 2016).

Marked changes in pore water profiles of other components also typically occur across the SMT (**Figure 2**). Because CH_4 is greatly depleted in ^{13}C (Paull et al., 2000), the conversion of CH_4 carbon to HCO_3^- carbon (**Equation 1**) induces a decrease in the $\delta^{13}C$ values of dissolved inorganic carbon (DIC) across the SMT (Torres et al., 2007; Holler et al., 2009; Yoshinaga et al., 2014). However, the magnitude of change becomes complicated because of excess HCO_3^- rising from below (Snyder et al., 2007; Chatterjee et al., 2011). Dissolved Ba^{2+} concentrations generally increase significantly just above the SMT. This is because solid barite ($BaSO_4$), a ubiquitous component of marine sediment on continental slopes (Dehairs et al., 1980; Dymond et al., 1992; Gingele and Dahmke, 1994), dissolves in the SO_4^{2-}-depleted pore water and dissolved Ba^{2+} then diffuses back across the SMT (Dickens, 2001; Riedinger et al., 2006; Nöthen and Kasten, 2011). Dissolved Ca^{2+} concentrations usually decrease across the SMT. This is due to authigenic carbonate precipitation resulting from the production excess HCO_3^- (Greinert et al., 2001; Luff and Wallmann 2003; Snyder et al., 2007). Importantly, though, dissolved NH_4^+

Biogeosciences Discuss., doi:10.5194/bg-2016-308, 2016
Manuscript under review for journal Biogeosciences
Published: 9 August 2016

concentrations exhibit no inflection across the SMT. This is because while decomposition of particulate organic matter generates NH_4^+, AOM does not (Borowski et al., 1996). In summary, pore water analyses at numerous locations demonstrate that characteristic pore water profiles delineate sites with significant CH_4, including gas hydrate, at depth (**Figure 2**).

3. Materials and Methods

3.1 The SWERUS-C3 Expedition, Leg 2

Between August 21 and October 5, 2014, Leg 2 of the SWERUS-C3 expedition sailed between Barrow, Alaska and Tromsø, Norway with *IB Oden*. This leg included four transects that cross the ESM continental slope (**Figure 3**). These transects were along Arlis Spur (TR-1), north of central East Siberia (TR-2), from close to Henrietta Island to the Makarov Basin (TR-3), and on the Amerasian side of Lomonosov Ridge (TR-4). Along each transect, scientific operations involved bathymetric mapping as well as sediment coring a series of stations. One station also was located on Lomonosov Ridge, near where this long bathymetric high intersects the ESM. Additionally, three days were spent at Herald Trough, a canyon on the shelf of eastern Siberia. Data obtained from the northern Lomonosov Ridge and Herald Canyon are not presented in this manuscript.

An array of coring techniques were used along each transect. In total, 50 sediment cores were collected at 34 coring stations. These included: multicore sets (22), gravity cores (23), piston cores (11), and kasten cores (2). The multicorer was an 8-tube corer built by Oktopus GmbH weighing 500kg. The polycarbonate liners were 60 cm long with a 10 cm diameter. The piston/gravity coring system was built by Stockholm University with an inner diameter of 10 cm. Trigger weight cores also were collected during piston coring. The different coring systems

Biogeosciences Discuss., doi:10.5194/bg-2016-308, 2016
Manuscript under review for journal Biogeosciences
Published: 9 August 2016

262 enabled sediment and pore water collection from the seafloor to upwards of eight to nine m
263 below the seafloor (mbsf).
264
265 *3.2 Core material*
266 Sediment physical properties (piston and gravity cores) were analyzed shipboard using a
267 Geotek Multi-Sensor Core Logger (MSCL) from Stockholm University. Measurements of the
268 gamma-ray derived bulk density, compressional wave velocity (p-wave), and magnetic
269 susceptibility were acquired at a down core resolution of one cm. Discrete samples (2-3 per
270 section) were collected for sediment index property measurements (bulk density, porosity, water
271 content and grain density). Grain density was measured using a helium displacement pycnometer
272 on oven-dried samples. Porosity profiles were generated using the smoothed (3-pt) MSCL-
273 derived bulk density (ρ_B) and the average grain density (ρ_g) from each core, where;
274 $$\varphi = \frac{(\rho_g - \rho_b)}{(\rho_b - \rho_f)}, \quad (5)$$
275 and a pore fluid density (ρ_f) of 1.024 g/cm^3 was assumed. In cases where 2 or more distinct
276 lithologic units existed within a core, the average grain density for each unit was used in this
277 calculation.
278 *3.3 Interstitial Water Collection*
279 Pore waters were collected using Rhizon samplers (Seeberg-Elverfeldt et al., 2005; Dickens
280 et al., 2007). Cores were cut into ~1.5 m long sections immediately on *Oden*'s deck, brought to
281 the geochemistry laboratory, and placed on precut racks. Laboratory temperature was a constant
282 22 °C. Sampling involved drilling holes through the core liner, inserting Rhizons into the
283 sediment core, and obtaining small volumes of pore water via vacuum and "microfiltration"
284 (**Figure 4**). An individual Rhizon consists of a hydrophilic membrane composed of a blend of

Biogeosciences Discuss., doi:10.5194/bg-2016-308, 2016
Manuscript under review for journal Biogeosciences
Published: 9 August 2016

polyvinylpyrrolidine and polyethersulfone (nominal pore size of 0.12 - 0.18 µm) connected to a tube. These are pushed into the sediment and, with negative pressure, the filament filters water into the syringe. The Rhizons were five cm porous flat tip male luer lock (19.21.23) with 12 cm tubing, purchased from Rhizosphere Research Products (www.rhizosphere.com).

In total, 529 pore water samples were collected in ~10 mL plastic syringes from 32 cores, which ranged from 0.16 to 8.43 m in length (**Table 1**). Rhizons in gravity and piston cores typically were spaced every 20 to 30 cm, although occasionally at five cm increments. Of the total, 456 samples obtained ~10 mL or more of pore water. Rhizon sampling from multicores took an average of 1.24 hr per sample, and ranged from 0.08 to 4.01 hr; for gravity and piston cores, the average sampling time was 11.28 hr, and ranged from 1.33 to 23.08 hr. Tabulated Rhizon flow rates averaged 12.72 mL/hr for multicores and 1.29 mL/hr for piston and gravity cores (**Table 2**). After considering the time to recover cores from the seafloor, the total time from core retrieval through sample collection averaged 1.95 hr for multicores and 14.65 hr for piston and gravity cores.

We highlight the above sampling times due to concerns about the fidelity of chemical analyses using Rhizon samplers in recent literature (Schrum et al., 2012; Miller et al., 2014). Since initial implementation of Rhizons in marine sediment cores (Seeberg-Elverfeldt et al., 2005; Dickens et al., 2007), they increasingly have been used to collect pore waters (e.g., Pohlman et al., 2008; Gao et al., 2010; Riedinger et al., 2014). This is for multiple reasons, including the capability for high-resolution sampling, the ease of sampling, and the minimal destruction of surrounding sediment (Dickens et al., 2007). However, concerns about using Rhizon samplers include CO_2 degassing during extraction (Schrum et al., 2012) or changes to pore water composition between core retrieval and water extraction. In the latter case, alteration

Biogeosciences Discuss., doi:10.5194/bg-2016-308, 2016
Manuscript under review for journal Biogeosciences
Published: 9 August 2016

of pore water chemistry may occur through reactions induced by elevated temperature, reduced pressure, evaporation, microbial activity or other processes.

In order to constrain possible changes in pore water chemistry over time, two experiments were performed onboard *IB Oden*. First, the temperature and pH of a piston core from Station 33 were continuously monitored at five discrete intervals over 24 hours. Probes, inserted into the sediment by drilling holes in the core liner, recorded data at five minute intervals (**Figure 5**). Second, for 46 samples (**Table 4**), after collection of the first 10 mL of pore water, the syringe was removed, and additional pore water was collected in a second (or third) syringe.

While in the shipboard laboratory, Rhizon samples were divided into six aliquots when sufficient water was available. This sample splitting led to 2465 aliquots of pore water in total, which then could be examined for different species and at different laboratories. Aliquots 1, 3, and 6 (below) were collected for all samples.

3.4 Interstitial Water Analyses

The first aliquot was used to measure total alkalinity using a Mettler Toledo titrator onboard *IB Oden*. Immediately after collection, 2 mL of pore water were diluted to 40 mL with milli-Q water and autotitrated with 0.005M HCl from the original pH to a pH of 5.4. A total of 15 spiked samples and 8 duplicates were analyzed onboard for quality control. Spiked samples were created by pipetting certified reference material (Batch 135; CRM) into milli-Q water. Results for spiked samples and duplicates are reported in **Table 3.**

The second aliquot was used to measure the $\delta^{13}C$ composition of DIC ($\delta^{13}C_{DIC}$). Septum sealed glass vials prepared with 100µL of 85% phosphoric acid and flushed with helium were prepared before the expedition. The analysis required approximately 40 µg of DIC in each pore

Biogeosciences Discuss., doi:10.5194/bg-2016-308, 2016
Manuscript under review for journal Biogeosciences
Published: 9 August 2016

water sample. Onboard alkalinity measurements were used to estimate the correct volume, and this amount was injected into the vials. Samples were sealed in boxes and refrigerated for the remainder of the cruise. Four field duplicates, two seawater standards, and a field blank were collected, stored, and analyzed with the samples. The $\delta^{13}C_{DIC}$ analyses were performed on a Gasbench II coupled to a MAT 253 mass spectrometer (both Thermo Scientific) at Stockholm University. The carbon isotope composition of DIC is reported in conventional delta notation relative to Vienna PeeDee Belemnite (VPDB). Results for field duplicates and standards are reported in **Table 2**. Standard deviation for the analyses of $\delta^{13}C_{DIC}$ was less than 0.1 per mille. The results for seawater standards collected onboard are given in **Table 3**.

The third aliquot was used to measure dissolved sulfur and metals. Approximately 3 mL of pore water were placed into acid washed cryovials. Samples were acid preserved with 10 µL ultrapure HNO^3. Additionally, 11 blind field duplicates and 2 field blanks were collected and processed in the same manner. Concentrations of Ba, Ca, Fe, Mg, Mn, S, and Sr were determined on an Agilent Vista Pro Inductively Coupled Atomic Emission Spectrometer (ICP-AES) housed in the geochemistry facilities at Rice University. Known standard solutions and pore fluid samples were diluted 1:20 with 18-MΩ water. Scandium was added to both standards and samples to correct for instrumental drift (emission line 361.383 nm). Wavelengths used for elemental analysis followed those indicated by Murray et al. (2000). Following initial analysis, an additional dilution, 1:80 with 18-MΩ water, was analyzed for Ca, Mg, and S. After every 10 analyses, an International Association of Physical Sciences (IAPSO) standard seawater spiked sample and a blank were examined for quality control. Relative standard deviations (RSD) from stock solutions are reported in **Table 3**.

Biogeosciences Discuss., doi:10.5194/bg-2016-308, 2016
Manuscript under review for journal Biogeosciences
Published: 9 August 2016

353 The fourth aliquot was used to measure dissolved ammonia (NH_4^+). This was carried out
354 shipboard via a colorimetric method similar to that presented by Gieskes et al. (1991). Set
355 volumes (100µL) of pore water were pipetted into 1 cm^3 plastic cuvettes and diluted with 900 µL
356 of milli-Q water. Two reagents (100 µL of A and 100 µL of B) were then pipetted into the
357 cuvettes. Reagent A was prepared by adding 35 g of trisodium citrate ($Na_3C_6H_5O_7$), 2.7 g of
358 phenol (C_6H_5OH), and 0.06 g of sodium nitroprusside ($Na_2[Fe(CN)_5NO]$) to 100 mL of milli-Q
359 water. Reagent B was prepared by dissolving 1.36 g of sodium hydroxide in 100 mL of milli-Q
360 water and adding 3 mL sodium hypochlorite (NaClO) solution. After the reagents were added,
361 solutions were mixed, and allowed to react for at least six but not more than 24 hours. Solutions
362 turned various shades of blue, which to relate to NH_4^+ concentration, and which were measured
363 by absorbance at 630 nm on a Hitachi U-1100 spectrophotometer. Five point calibration curves
364 (0 to 200 µM) were measured before each sample set and corrected using VKI standard (QC
365 RW1; www.eurofins.dk; **Table 3**).
366 The fifth aliquot was used to measure dissolved phosphate (PO_4^{3-}). The method of
367 preparation also followed that given by Gieskes et al. (1991). The remainder of the pore water
368 (generally between 1 and 3mL) was added to milli-Q water to a sum of 10 mL. Two reagents
369 were then added to the solution to react with phosphate (200 µL of A and B). Reagent A was
370 prepared by first making three solutions: eight grams of ammonium molybdate ($(NH_4)_2MoO_4$)
371 were added to 80 mL of milli-Q water, 50 mL of concentrated sulfuric acid were added to 150
372 mL of milli-Q water, and 0.01 g of potassium antimonyl tartrate hydrate ($C_8H_4K_2O_{12}Sb_2 \bullet XH_2O$) were added to 10 mL of milli-Q water. Then, 30 mL of the ammonium molybdate
374 solution were added to 90 mL of the sulfuric acid solution, and five mL potassium antimonyl
375 tartrate solution was slowly added dropwise. Reagent B was created by dissolving 10 g of

Biogeosciences Discuss., doi:10.5194/bg-2016-308, 2016
Manuscript under review for journal Biogeosciences
Published: 9 August 2016

ascorbic acid in 50 mL of milli-Q water. After the samples were prepared, reagent A and B were added, mixed, and allowed to react for 10 but not more than 30 minutes. Solutions turned various shades of blue, which to relate to PO_4^{3-} concentration, and which were then measured at an absorbance of 880 nm on the above spectrophotometer. Five point calibration curves (0 to 50 µM) were measured before each sample set and corrected using VKI standard (QC RW1; www.eurofins.dk; **Table 3**).

In cases of excess sample, an additional aliquot was collected to test for dissolved hydrogen sulfide. Approximately 2 mL of pore water was placed into a cryovial, and 200 µL of a 2.5% Zn-acetate ($Zn(C_2H_3O_2)_2$) solution was added. Given the extremely low solubility of ZnS, a white precipitate should form in the presence of even very low H_2S concentrations (Cline, 1969; Goldhaber, 1974).

4. Results

4.1 Generalities

With the large number of pore water measurements (**Table 1**) we begin with some generalities regarding the results. We plot pore water concentration profiles along each transect collectively (**Figures 6 - 10**), irrespective of coring device or water depth, although clear variance in pore water chemistry exists between stations for some dissolved species (e.g., Fe).

Most species display "smooth" concentration profiles with respect to sediment depth (**Figures 6 - 10**). That is, concentrations of successive samples do not display a high degree of scatter. This is expected for pore water profiles in sediment where diffusion dominates (Froelich et al., 1979; Klump and Martens 1981; Schulz, 2000). However, as best seen for dissolved species whose concentrations do not appreciably change over depth (e.g., Ba^{2+} and Ca^{2+}) scatter

Biogeosciences Discuss., doi:10.5194/bg-2016-308, 2016
Manuscript under review for journal Biogeosciences
Published: 9 August 2016

399 exists beyond that predicted from analytical precision. This scatter has a weak positive
400 correlation with increased sampling time, which can be shown by comparing time to a deviation
401 in concentration (**Figure 11**). The latter is defined by:

402 $$\Delta X = X_{Measured} - X_{Predicted}\ , \quad (6)$$

403 where X is the species of interest, and $X_{Predicted}$ is the concentration of X determined from the
404 linear best fit line of a concentration profile.

405 A method detection limit (MDL) for each species can be determined by the following
406 equation:

407 $$MDL = \left(\frac{C_{High} - C_{Low}}{I_{High} - I_{Low}}\right) 3\sigma\ , \quad (7)$$

408 where C = concentration and I = intensity (counts per second on the ICP-AES). The MDLs were
409 as follows: Ba = 0.01 µM, Ca = 0.08 µM, Fe = 5.9 µM, Mg = 0.22 µM, Mn = 0.24 µM, S = 1.2
410 µM, Sr = 0.01 µM. On all plots, for reference, we place dashed lines for values of IAPSO
411 seawater standard (Alkalinity = 2.33 mM, Ba = 0.00 mM, Ca = 10.28 mM, Fe = 0.00 mM, Mg =
412 53.06 mM, Mn = 0.00 mM, S = 28.19 mM, Sr = 0.09 mM, NH_4 = 0.00 mM, HPO_4 = 0.00 mM).
413 Pore water profiles generated from ACEX cores (Backman et al., 2009) also are shown for
414 comparison.

415

416 *4.2 Porosity and Sampling Time*

417 Measured porosity values of piston and gravity cores generally decrease with depth from
418 80% or greater at the mudline to around 60% at eight mbsf (**Figure 12a**). Over the first 0.1 m,
419 porosity decreases steeply, by an average of 6.8%. From 0.2 to 8.0 m, porosity decreases much
420 more gradually, by an average of 1.3% every meter. The 1σ deviation in porosity between all
421 stations typically ranges between 6 and 10% at any given depth.

Biogeosciences Discuss., doi:10.5194/bg-2016-308, 2016
Manuscript under review for journal Biogeosciences
Published: 9 August 2016

Sampling time inversely relates to porosity (**Table 2**). Multicore rhizon extraction rates (**Table 2**) averaged 12.72 mL/hr while gravity and piston cores averaged 1.29 mL/hr. This flow rate generally decreased with depth. Across all data from all cores, a first-order relationship between depth (z) and extraction rate (ER) can be expressed as $ER = 4.4911z^{-1.512}$ ($R^2 = 0.789$; **Figure 12b**). The extraction rate correlated with depth more closely than with porosity (**Figure 12c**). The porosity (ϕ)-extraction rate relationship, expressed as $ER = 21.718(\phi)^{8.161}$ had an $R^2 = 0.631$.

4.3 Physiochemical Conditions During Rhizon Sampling

For the five sections from Station 33 examined for changes in physiochemical conditions, temperature rose from ~2°C upon initial measurement to between 16.9 and 18.4 °C within 24 hours (**Figure 5**). In general, the shallow sections increased faster than the deeper sections. Initial pH decreased with depth (0.05 mbsf = 7.79 units, 1.86 mbsf = 7.71 units, 4.80 mbsf = 7.39 units, and 6.30 mbsf = 7.19 units). Over the same time interval, pH decreased significantly in all core sections, by an average of 0.25 units, with a range between 0.18 and 0.38 units (**Figure 5**). Note, however, that pH dropped by 0.3 units at ~20 hrs in one of the pH profiles (Section 2, 1.86 mbsf). This may be due to a temporary crack in the sediment core created by removing pore water through rhizon sampling, although no crack was observed when the core section was split.

In total, 46 of the 68 Rhizon sampling depths at Station 28 enabled collection of multiple water samples (**Table 4**). This included "second generation" samples, where beyond the first ~10 mL, another 1 to 10 mL were obtained, as well as three "third generation" samples, where beyond the first ~20 mL, another 1 to 10 mL were obtained. The sample depths which did not yield enough pore water for a "second generation" tended to be deeper (16 of 22 were in the

Biogeosciences Discuss., doi:10.5194/bg-2016-308, 2016
Manuscript under review for journal Biogeosciences
Published: 9 August 2016

445 deepest section). Relative to the initial 10mL of pore water, alkalinity increased in 43 of the
446 second generation samples, and in all three of the third generation samples by an average 0.15
447 mM (4.1% increase). Interestingly, no statistically significant changes in concentrations of
448 phosphate, ammonia or any dissolved metal were observed.
449
450 *4.4 Alkalinity and $\delta^{13}C$*
451 Alkalinity concentrations increase with depth in all cores (**Figures 6 - 10**). Moreover, in
452 most cases, the rise is nearly linear. Across all stations on the four transects, alkalinity increases
453 by an average of 0.51 mM/m, although variance exists between mean gradients for each transect
454 (Tr1 = 0.46 mM/m, Tr2 = 0.34 mM/m, Tr3 = 0.91 mM/m, and Tr4 = 0.44 mM/m) and by station
455 along each transect. Overall, the rise in alkalinity at these 15 stations ranges from 0.30 to 0.98
456 mM/m. The Lomonosov Ridge station differs (**Figure 10**), as alkalinity increases much faster
457 with depth (1.86 mM/m).
458 Concave-down δ^{13}C-DIC profiles characterize pore waters at all stations (**Figures 6 - 10**).
459 The decrease in δ^{13}C-DIC changes most rapidly near the seafloor. Across all stations along the
460 four transects, pore water δ^{13}C-DIC values decrease from near zero close to the mudline at an
461 average of -3.6 ‰/m. Again, significant variance in mean gradients occurs according to transect
462 (Tr1 = -3.3 ‰/m, Tr2 = -3.0 ‰/m, and Tr3 = -4.7 ‰/m) and according to station on each
463 transect. The range in average δ^{13}C-DIC value gradients across all stations is -2.7 to -4.9 ‰/m.
464 As with alkalinity, the δ^{13}C-DIC profile at the Lomonosov Ridge station differs, with values
465 decreasing by 5.6 ‰/m, such that 8 mbsf, δ^{13}C-DIC approaches -45 ‰. In summary, a basic
466 relationship exists between higher alkalinity and lower δ^{13}C-DIC across all stations.
467

Biogeosciences Discuss., doi:10.5194/bg-2016-308, 2016
Manuscript under review for journal Biogeosciences
Published: 9 August 2016

468 *4.5 Sulfur and sulfate*

469 No sulfide was detected by smell or with addition of Zn-acetate in any pore water sample.
470 Molar concentrations of total dissolved sulfur should, therefore, represent those of dissolved
471 SO_4^{2-}. Along the four transects, dissolved S concentrations decrease with depth at all stations
472 (**Figures 6 – 9**). The sulfur concentration in the shallowest sample varied from 27.29 to 30.58
473 mM and averaged 28.70 mM. From these "seafloor" values, concentrations decrease by an
474 average 0.69 mM/m, again with variance according to transect (Tr1 = -0.58 mM/m, Tr2 = -0.57
475 mM/m, Tr3 = -1.09 mM/m; and Tr4 = -0.60 mM/m) and station along each transect. The S
476 gradients across all stations along the ESM slope range from -0.41 to -1.13 mM/m. Total
477 dissolved S at the Lomonosov Ridge station decreased faster than at any of the other stations (-
478 1.92 mM/m). Importantly, decreases in dissolved S are similar in magnitude to increases in
479 alkalinity at each station. Indeed, the molar ratio of alkalinity increase to sulfate decrease (-
480 ΔAlkalinity/ΔS) is 0.98 (**Figure 13a**).

481

482 *4.6 "Nutrients": Phosphate and Ammonia*

483 Often, in discussions of pore water chemistry, dissolved phosphate (HPO_4^{2-}) and ammonia
484 (NH_4^+) are classified as "nutrients", although the connotation derives from the fact that these two
485 species arise through the oxidation of POM in the sediment (Berner, 1977). The C:N:P molar
486 ratio, known as the "Redfield Ratio", of initial POM is approximately 106:16:1 (Redfield, 1958;
487 Takahashi, 1985). Therefore, assuming mass balance, dissolved "nutrients" are used as reference
488 for the amount of POC consumed through microbial oxidation. Importantly, concentrations of
489 HPO_4^{2-} and NH_4^+ are near or below detection in samples immediately below the seafloor
490 (**Figures 6 -10**).

Biogeosciences Discuss., doi:10.5194/bg-2016-308, 2016
Manuscript under review for journal Biogeosciences
Published: 9 August 2016

With depth, concentrations of dissolved HPO_4^{2-} typically increase, reach a subsurface maximum, and then decrease (**Figure 6 – 10**). With available data, a more pronounced maximum generally occurs at stations with relatively shallow water depth. For example, and within the spatial resolution of samples, consider the peak in HPO_4^{2-} concentrations at four stations. At the two shallow stations, S12 (384 m) and S22 (367 m) the HPO_4^{2-} maxima are, 73 µM (1.91 m) and 18 µM (0.66 m), respectively at the two deeper stations, S17 (977 m) and S14 (733 m), the HPO_4^{2-} maxima are only 6.7 µM (1.76 m) and 7.1 µM (2.33 m) respectively. The station on Lomonosov Ridge (S31) has a high in HPO_4^{2-} concentration of 76 µM at 1.02 m below the mudline. In general, stations with more pronounced HPO_4^{2-} maxima also have greater increases in alkalinity with depth.

By contrast, dissolved NH_4^+ profiles rise almost linearly with depth, but with slight concave-down curvature. Similar to dissolved HPO_4^{2-} profiles, NH_4^+ concentrations increase with depth fastest at stations with shallower water depth (although we note an exception for Tr2). Across stations along the four transects, pore water NH_4^+ concentrations increase with depth on average by 38.69 µM/m, with a range from 11.28 to 76.08 µM/m. Along each transect, the average NH_4^+ gradients are as follows: Tr1 = 43.02 µM/m, Tr2 = 17.38 µM/m, Tr3 = 68.97 µM/m, and Tr4 = 29.04 µM/m.

The HPO_4^{2-}, NH_4^+, and alkalinity profiles relate to one another statistically, although with distinction. The concentration relationship of alkalinity and ammonium ion can be expressed by a second order polynomial ($[NH_4^+] = -0.003[Alk]^2 + 0.105\,[Alk] - 0.253$; **Figure 13b**) with an average molar ratio ($\Delta Alk/\Delta NH_4^+$) of 14.69. All stations have a C:N ratio in pore waters more than the Redfield Ratio of 6.625 (**Figure 14**). The molar ratio of alkalinity and phosphate ion ($\Delta Alk/\Delta HPO_4^{2-}$) averages 55.72 for all stations. This means that all stations have an average C:P

Biogeosciences Discuss., doi:10.5194/bg-2016-308, 2016
Manuscript under review for journal Biogeosciences
Published: 9 August 2016

514 ratio less than 106. Overall, a consistent pattern emerges between changes in NH_4^+, and
515 alkalinity, but one that deviates significantly from Redfield ratio. Interestingly, the C:N ratio
516 appears to vary significantly across transects. This ratio increases from Tr1 (8.61-11.22), Tr3
517 (12.5-18.14), Tr2 (17.53-18.55), to the Lomonosov Ridge station (22.62). The C:P ratio followed
518 a similar pattern, generally increasing from east to west: Tr1 (16.57-74.70), Tr2 (26.32-92.04),
519 Tr3 (26.29-86.34), and Tr4 (52.18-124.35).
520
521 *4.7 Metals*
522 At most stations, dissolved Ba concentrations increase nonlinearly from values at or below
523 detection limit (0.01 µM) near the seafloor to generally constant values (0.6 – 0.7 µM) within 0.8
524 m below the seafloor. However, at several stations, dissolved Ba concentrations remained at or
525 below the detection limit for all samples.
526 Overall, dissolved Ca, Mg, and Sr concentrations decrease slightly with depth (**Figures 6 -**
527 **10**). Across stations along the four transects, Ca concentrations drop on average between -0.094
528 and -0.122 mM/m (Tr1), between -0.092 and -0.093 mM/m (Tr2), between -0.092 and -0.101
529 (Tr3), and -0.075 mM/m (Tr4). Magnesium concentrations also drop, the average change being
530 between -0.430 and -0.481 mM/m (Tr1), between -0.274 and -1.319 (Tr2), between -0.863 and -
531 0.942 mM/m (Tr3), and -0.467 mM/m (Tr4). Strontium concentrations decrease by an average
532 amount of 0.3 µM/m, considering all stations along the four transect stations (Tr1 = 0.5 µM/m,
533 Tr2 = 0.3 µM/m, Tr3 = 0.1 µM/m, and Tr4 = 0.1 µM/m). The station on Lomonosov Ridge again
534 stands apart. At this location, the decreases in dissolved Ca, Mg, and Sr are 0.27 mM/m, 1.24
535 mM/m, and 0.50 µM/m, respectively.

Biogeosciences Discuss., doi:10.5194/bg-2016-308, 2016
Manuscript under review for journal Biogeosciences
Published: 9 August 2016

The profiles of dissolved Mn and Fe are spatially complicated. Generally, profiles show a broad rise in concentration and subsequent fall at deeper depth. Some stations have a maxima in dissolved Mn (Stations S12 (135 µM at 5 m), S28 (66 µM at 3.1 m), and Lomonosov Ridge (86 µM at 1.3 m), where concentrations decrease below. At other stations, Mn concentrations are still increasing at the lowest depth. Iron concentrations are generally below the detection limit at or near the mudline, and begin increasing around 2.5 – 3.5 m reaching concentrations upward of 20 µM.

5. Discussion

5.1 Flow Rates from Rhizons

Pore water flow rate drops quasi-exponentially with depth (**Figure 12b**), similar to what was documented on ACEX (Dickens, 2007). This probably results from the decrease in porosity (and presumably permeability) with depth (**Figure 12c**). Given that individual Rhizons have similar vacuum to pull the water, a decrease in porosity and permeability means a slower flow (Domenico and Schwartz, 1998).

5.2 Fidelity of Rhizon Pore Water Measurements

Researchers have employed multiple methods to extract pore waters from marine sediments over the last few decades (Seeberg-Elverfeldt et al., 2005). As the rhizon technique remains relatively novel, the accuracy and precision of analyses obtained through this approach warrant consideration before discussing the results. This issue arises particularly because of the two aforementioned papers questioning the fidelity of pore water records generated through rhizon sampling.

Biogeosciences Discuss., doi:10.5194/bg-2016-308, 2016
Manuscript under review for journal Biogeosciences
Published: 9 August 2016

559 Schrum et al. (2012) compared dissolved species collected by whole round squeezing and
560 rhizons. They observed very subtle but consistent (0.06 to 0.8 mM) offsets to lower alkalinity in
561 Rhizon samples, and hypothesized that this reflected CO_2 degassing during extraction. For
562 example, the release of gas during filtering under vacuum conditions might increase, leading to
563 precipitation of $CaCO_3$, and ultimately a drop in alkalinity. They noted, though, that rhizons
564 seemed to provide accurate measurements for nutrients and metals.
565 Miller at al. (2014) compared chloride concentrations, oxygen isotopes, and hydrogen
566 isotopes in pore waters collected from whole round squeezing and rhizons. The rhizon samples
567 appeared to have higher [Cl^-] and greater enrichments in heavier isotopes (^{18}O and D). The
568 authors suggested some combination of water absorption onto the hydrophilic membrane, ion
569 exclusion and isotope fractionation due to clay ultrafiltration, and water evaporation during
570 degassing as possible sources for these offsets.
571 Rather than an issue with Rhizon sampling per se, an alternative explanation for analytical
572 discrepancies lies with collection time. A lengthy time between core retrieval and final pore
573 water collection could allow for changes in physiochemical conditions, which might relate to
574 evaporation and carbonate precipitation. Our experiments show that significant differences in the
575 chemical environment of cores occur during rhizon sampling. Consider the temperature (**Figure**
576 **5a**) and pH (**Figure 5b**) evolution over 24 hours for the five core sections from station S33 that
577 were analyzed. Note that the time to recover, to cut, and to transport these sections from the ship
578 deck to the geochemistry laboratory (total 1.71 hrs) was similar to that involved for other
579 samples (**Table 1**). Thus, we consider results from these cores representative.
580 Many authors have observed variations in pore water pH, DIC, alkalinity, and Ca^{2+} values
581 over time (e.g., Gieskes, 1974; Paull et al., 1996; Wang et al., 2010; Sauvage, 2013). The

Biogeosciences Discuss., doi:10.5194/bg-2016-308, 2016
Manuscript under review for journal Biogeosciences
Published: 9 August 2016

582 changes in sections from S33 clearly indicate that physiochemical conditions within the core
583 change significantly within 24 hours. The ~15 °C increase will alter inorganic solid-liquid
584 equilibrium conditions (de Lange et al., 1992), and should increase microbial respiration (Sander
585 and Kalff, 1993). The nominal ~0.25 drop in pH implies a reduction in alkalinity. Interestingly,
586 though, this appears opposite of results from sequential sampling, where each progressive
587 "generation" of pore water had greater alkalinity.

588 One issue is location. The pH sondes were always more than 10 cm from the nearest
589 rhizon. Although it is possible that the Rhizon's negative pressure in the sediment is
590 compensated by O_2/air increasing respiration, previous experiments on rhizon flow (Seeberg-
591 Elverfeldt et al., 2005; Dickens et al., 2007) indicate that rhizons generally pull water from <3
592 cm along the core. Thus, water masses adjacent to pH meters were likely "out-of
593 communication" with those being sampled by the rhizons. We suggest that at least two factors
594 effect chemistry: (1) temperature and pH (and pressure) of pore waters change with time after
595 core retrieval; and, (2) pore water chemistry evolves during water removal.

596 The observed evolution of pore water chemistry may be related to increasing temperature
597 and possible introduction of atmospheric air via the Rhizon drill hole each time the syringe was
598 removed. As temperature increases, greater microbial activity may drive pH down by increasing
599 CO_2 concentration. Additionally, removing the syringe may have provided opportunity for
600 atmospheric air to enter the sediment through the filament. As the pH decreased, carbonate
601 dissolved, increasing HCO_3^- concentration in the pore water. The Rhizons continually applied
602 additional negative pressure. However, as stated previously, the pH sondes were sufficiently far
603 from the Rhizons to be affected by pore water extraction.

Biogeosciences Discuss., doi:10.5194/bg-2016-308, 2016
Manuscript under review for journal Biogeosciences
Published: 9 August 2016

As clearly documented here and in other works (Seeberg-Elverfeldt et al., 2005; Dickens et al., 2007; Pohlman et al., 2008), rhizon sampling can lead to "smooth" concentration profiles for multiple dissolved species, including alkalinity (**Figures 6 – 10**). The concerns raised about rhizon sampling may be valid for dissolved components when concentration gradients are low. For example, Schrum et al. stressed alkalinity differences of 0.06 to 0.8 mM, but the total alkalinity range in this study was 1.80 and 14.58 mM. A similar finding occurs in the dissolved Ca^{2+} and Ba^{2+} profiles of this study, where adjacent samples deviate by amount greater than analytical precision (**Table 3, Figure 11**). However, when the signal to noise ratio become high, as true with most dissolved components at most stations (**Figures 6 – 10**), the rhizon sampling renders pore water profiles with well defined concentration gradients that can be interpreted in terms of chemical reactions and fluxes.

5.3 Reading the Pore Water Profiles

Pore water profiles in most marine sediment express solute fluxes resulting from chemical reactions, sediment properties, and diffusion (Berner, 1980; Berg et al., 1998). Within 10 m of the seafloor, where temperature and the diffusion coefficient change minimally, depth intervals having inflections in the concentration gradient (dC/dz) generally represent zones where production or consumption of dissolved components occur (ΔJ), or where porosity (ϕ) changes significantly (**Equation 2**). Importantly, excepting areas of the seafloor with strong fluid flow (e.g., mud volcanoes, cold seeps), methane charged sediments along continental margins have very predictable pore water profiles.

As previously emphasized, numerous studies demonstrate that a prominent SMT characterizes shallow sediment in locations with high methane concentrations in underlying

Biogeosciences Discuss., doi:10.5194/bg-2016-308, 2016
Manuscript under review for journal Biogeosciences
Published: 9 August 2016

627 strata. Moreover, inflections in pore water SO_4^{2-}, alkalinity, δ^{13}C-DIC values, and hydrogen
628 sulfide consistently occur across this geochemical horizon (**Figure 2**). This is because AOM
629 consumes SO_4^{2-} and produces ^{13}C-depleted HCO_3^- and HS^- (**Equation 1**). The overall
630 geochemistry is best understood by considering fluxes (Borowski et al., 1996; Berg et al., 1998;
631 Chatterjee et al., 2011). Across the SMT, upward migrating methane of some flux (JCH$_4$) reacts
632 with downward diffusing SO_4^{2-} of equal flux but opposite sign ($-J$SO$_4^{2-}$). This leads to a sharp
633 concave-down inflection in SO_4^{2-} concentrations (i.e. the SMT), with the depth driven by JCH$_4$.
634 Fluxes of HCO_3^- (JHCO$_3^-$) and HS^- (JHS$^-$) of similar magnitude enter pore water, but are
635 expressed differently in pore water profiles. In general, the input of ^{13}C-depleted HCO_3^-
636 contributes to already ^{13}C-enriched HCO_3^- concentrations, produced during methanogenesis
637 deeper in the sediment column. The consequence is a steep rise in HCO_3^- concentrations with
638 depth, but having a positive kink across the SMT, where a coincident drop in the δ^{13}C-DIC
639 values occur. The input of HS^- diffuses upward and downward, where it reacts with dissolved Fe
640 or sedimentary phases. The consequence is a "bell shaped" HS^- pore water profile with the
641 maxima at the SMT.

642 Good examples of where such pore water chemistry is documented include: Baltic Sea
643 (Jørgensen et al, 1990), Black Sea (Jørgensen et al, 2004), Blake Ridge (Paull et al., 2000;
644 Borowski et al., 2001), Cariaco Trench (Reeburgh, 1976), Cascadia Margin (Torres and Kastner,
645 2009), Gulf of Mexico (Kastner et al., 2008a; Hu et al., 2010; Smith and Coffin, 2014), Hydrate
646 Ridge (Claypool et al., 2006), offshore Namibia (Niewohner et al., 1998), offshore Peru
647 (Donohue et al., 2006), South China Sea (Luo et al., 2013; Hu et al., 2015), and Sea of Japan
648 (Expedition Scientists, 2014). In any case, through use of **Equation 2**, fluxes of dissolved ions,
649 and by inference dissolved CH$_4$, can be calculated from measured pore water concentration

Biogeosciences Discuss., doi:10.5194/bg-2016-308, 2016
Manuscript under review for journal Biogeosciences
Published: 9 August 2016

profiles with knowledge of porosity and sedimentary diffusion constants (e.g., Niewohner et al., 1998). At sites with abundant methane in the upper few hundred meters, notably including sites with gas hydrate, estimated values for J_{CH_4} and $-J_{SO_4^{2-}}$ are universally high (**Table 4**).This includes sites in the Beaufort Sea, 154.8 mol/m^2-kyr (Coffin et al., 2013), 102 mol/m^2-kyr (Umitaka Spur; Snyder et al., 2007), 86.2 mol/m^2-kyr (Hikurangi Margin; Coffin et al., 2007), 362.0 mol/m^2-kyr (Chilean Margin; Coffin et al., 2006), 162.5 mol/m^2-kyr (Argentine Basin; Hensen et al., 2003; **Figure 15**). Methane above gas hydrates can migrate upward even faster through advective bubble ebullition at cold seeps (Joye et al., 2004).

5.4 General Absence of Methane

Direct measurements of dissolved CH_4 in deep-sea sediment are complicated (Claypool and Kvenvolden 1983). During core retrieval and depressurization, gas ebullition occurs, which leads to significant CH_4 loss from pore space. Interestingly, however, in sediments containing high CH_4 concentrations and recovered through piston coring, gas release typically generates obvious sub-horizontal cracks that span the core between the liner. No such cracks were documented in any of the cores.

Excluding Station St31 on the southern Lomonosov Ridge (discussed below), there is no indication of a shallow SMT. Interstitial water sulfur concentrations do not drop below 22.78 mM within the upper 8 m. In fact, calculated downward SO_4^{2-} fluxes, as inferred from sulfur concentration gradients (**Table 4**) range from -1.8 to -9.2 mol/m^2-kyr for all stations except Station S31. For comparison, with a temperature of 2 °C (**Figure 5a**) and measured porosities (**Figure 12a**), even an SMT at six mbsf would imply SO_4^{2-} flux of -40 mol/m^2-kyr.

Biogeosciences Discuss., doi:10.5194/bg-2016-308, 2016
Manuscript under review for journal Biogeosciences
Published: 9 August 2016

672 Given the lack of HS^- and the measured pH at Station S33 (**Figure 5**), alkalinity should
673 closely approximate HCO_3^- concentrations (**Equation 4**). Estimated HCO_3^- fluxes do not exceed
674 6.8 mol/m2-kyr at any station east of the Lomonosov Ridge (**Table 4**). For comparison, when
675 alkalinity gradients are used to estimate $JHCO_3^-$ at sites with abundant CH_4 at depth, values
676 generally exceed 30 mol/m^2-kyr above the SMT (**Table 4**). These extreme fluxes arise because
677 methanogenesis in deeper sediment drives an upward flux of HCO_3^- (**Figure 2**), and because
678 AOM also contributes HS^- to pore water at the SMT (**Equation 1**).
679 The δ^{13}C-DIC values of pore water decrease with depth at all stations, almost in concert
680 with the rise in alkalinity. However, other than Station S31, the lowest value of δ^{13}C-DIC is -
681 25.23 ‰ at 5.5 m at Station S22 (**Figure 8**). This is interesting because a series of microbial
682 reactions utilizing particulate organic matter (POM) can lead to higher alkalinity and lower δ^{13}C-
683 DIC values in pore water (Chatterjee et al., 2001). The most important of these reactions is
684 organoclastic sulfate reduction, which can be expressed as (Berner, 1980; Boudreau and
685 Westrich, 1984):

686 $$2^{12}CH_2O + SO_4^{2-} \rightarrow H_2S + 2H^{12}CO_3^-\ , \qquad (8)$$

687 where again the ^{12}C superscript indicates depletion in ^{13}C. Notably, this reaction has a 2:1
688 relationship between C and S fluxes, rather than the 1:1 ratio of AOM (**Equation 1**).
689 As emphasized previously, methane-charged sediment sequences do occur on continental
690 slopes in the Arctic. Of particular interest to this study are locations in the Beaufort Sea, where
691 indications for gas hydrate manifest on seismic profiles (Grantz et al., 1976; Grantz et al., 1982;
692 Weaver and Stewart, 1982; Hart et al., 2011; Phrampus et al., 2014), and pore water profiles
693 have been generated using shallow piston cores (Coffin et al., 2013). Striking contrasts exist
694 between pore water profiles of the Beaufort Sea and those of the ESM (**Table 4; Figure 15**). In

Biogeosciences Discuss., doi:10.5194/bg-2016-308, 2016
Manuscript under review for journal Biogeosciences
Published: 9 August 2016

695 the Beaufort Sea, there are moderate to high downward sulfate and upward methane fluxes (1.9
696 to 154.8 mol/m^2-kyr), shallow SMTs (6.29 to 1.06 mbsf), high DIC fluxes between the SMT and
697 the mudline (46.3 to 242.6), and negative δ^{13}C-DIC values at SMT's (≈ -20‰).
698
699 *5.5 Special Case "Lomonosov Ridge Station"*
700 Station 31 on the Lomonosov Ridge (**Figure 10**) differs from all other stations examined
701 in this study. Here, pore water chemistry profiles hint at CH_4 in pore space within shallow
702 sediment. Extrapolation of the dissolved sulfur profile suggests an SMT at approximately 13.9
703 m. Such a depth lies within the range common for locations with AOM (D'Hondt et al., 2002),
704 notably including well studied sites on Blake Ridge (Borowski et al., 1999). Similar to some sites
705 with CH_4, the δ^{13}C-DIC values become very "light"; indeed, the value at the base of the core, -
706 43.54, almost necessarily implies CH_4 oxidation and a shallow SMT. Comparably steep
707 alkalinity (1.6 mM/m) and NH_4 gradients (60.4 μM/m) also characterize other sites with CH_4
708 near the seafloor. However, an issue concerns reduced sulfur produced via AOM (**Equation 1**).
709 One might expect evidence of HS^- migrating from below (**Figure 2**), but none was detected.
710 A comparison of published DIC fluxes, SO_4^{2-} fluxes, and SMT depths (**Table 4**) reveals
711 fluxes decrease exponentially with SMT depth (**Figure 15**). A fundamental relationship exists
712 when one considers that CH_4 flux controls SMT depth (**Equation 1**; **Figure 2**). The modest
713 SO_4^{2-} flux (-13.9 mol/m^2-kyr) and alkalinity flux (11.3 mol/m^2-kyr) of the Lomonosov Ridge
714 station fits quite well with literature values of similar SMT depth. For example, Hensen et al.
715 (2003) calculated a -14.69 mol/m^2-kyr SO_4^{2-} flux for a site with an SMT at 14 m in the Argentine
716 Basin. Berg (2008) calculated a SO_4^{2-} flux of -8.05 mol/m^2-kyr for a site with an SMT at 16 m at
717 the Costa Rican Margin.

Biogeosciences Discuss., doi:10.5194/bg-2016-308, 2016
Manuscript under review for journal Biogeosciences
Published: 9 August 2016

718

719 *5.6 Other Chemistry*

720 A well-documented sequence of reactions characterize shallow marine sediment
721 (Froelich et al., 1979; Berner, 1980). Microbial communities preferentially utilize the most
722 energetically favorable oxidant available (Froelich et al., 1979; D'Hondt et al., 2002). Thus, with
723 increasing depth below the seafloor, a near universal order of oxidation/reduction reactions arise:
724 aerobic respiration, denitrification, manganese reduction, nitrate reduction, iron reduction, sulfate
725 reduction, and finally methanogenesis. Importantly, these reactions impact pore water chemistry
726 and the depths of zones dominated by these reactions generally depend on the supply of POM to
727 the seafloor.

728 Many of the cores collected along the slope of the ESM appear to terminate in the zone of
729 metal oxide reduction. This is because, at most stations, Mn and Fe profiles are still increasing at
730 the bottom of the sampled interval (**Figure 6-10**). The relatively deep depths of metal oxide
731 reduction are consistent with a relatively low input of POM to the seafloor, and moreover
732 generally contrast with sites of high CH_4 concentrations in shallow sediment. From a simple
733 perspective, there may be insufficient POC to drive methanogenesis near the seafloor.

734 The station on the Lomonosov Ridge again stands apart. Here, Mn and Fe concentrations
735 reach maxima at 1.3 mbsf and 0.5 mbsf, respectively, and decrease below. Thus, complete
736 consumption of Mn and Fe occurs in the upper few meters, and methanogenesis could be
737 occurring below 13.9 mbsf.

738

739 *5.7 Signatures of AOM and Organoclastic Sulfate Reduction*

Biogeosciences Discuss., doi:10.5194/bg-2016-308, 2016
Manuscript under review for journal Biogeosciences
Published: 9 August 2016

740 Some authors have used changes in DIC and SO_4^{2-} concentrations between the seafloor
741 and the SMT to infer the relative importance of AOM and organoclastic sulfate reduction (OSR)
742 in marine sediments (Kastner et al. 2008b; Luo et al. 2013; Hu et al. 2015). The idea is can be
743 expressed by comparing $\Delta(DIC+Ca^{2+}+Mg^{2+})$ and ΔSO_4^{2-}, where Ca^{2+} and Mg^{2+} are included to
744 account for loss of DIC via carbonate precipitation. The rationale lies in the fact that the C:S
745 ratio for AOM is 1:1 (**Equation 1**), whereas the C:S ratio for OSR is 2:1 (**Equation 8**).
746 However, this approach neglects two considerations: (1) changes in concentration do not directly
747 relate to fluxes, because of differences in diffusivities of various ionic species, and, (2) a flux of
748 HCO_3^- from below the SMT can augment the DIC produced from AOM or OSR at or above the
749 SMT (Dickens and Snyder, 2009). Thus, changes in alkalinity relative to SO_4^{2-} often exceed 1:1,
750 even at locations completely dominated by AOM (Chatterjee et al., 2011).
751 Rather than just comparing changes in C:S molar ratios, to interrogate the importance of
752 the two reactions, one might also incorporate δ^{13}C-DIC value. This is because δ^{13}C-DIC values
753 and the depth of DIC production differ considerably for AOM, OSR and methanogenesis at
754 many locations. We generate a figure expressing these relationships at multiple sites (**Figure 16**),
755 where the y-axis is:

$$\frac{\Delta(DIC + Ca^{2+} + Mg^{2+})}{\Delta(SO_4^{2-})}, \quad (9)$$

756 and the x-axis is: DIC*δ^{13}C-DIC. The C:S ratios of dissolved species lie above 1:1 at most
757 locations, regardless of whether CH_4 exists in shallow sediment However, sites with CH_4 have
758 considerably more negative DIC*δ^{13}C-DIC values Notably, all stations from the ESM, except
759 S31 on the Lomonosov Ridge, have modest DIC*δ^{13}C-DIC values.
760 Two basic models help to explain the relationships in **Figure 16**. The first model assumes
761 all SO_4^{2-} consumption occurs through OSR; whereas the second model assumes that SO_4^{2-}

Biogeosciences Discuss., doi:10.5194/bg-2016-308, 2016
Manuscript under review for journal Biogeosciences
Published: 9 August 2016

762 consumption occurs via AOM and OSR, but DIC from methanogenesis also migrates upward
763 from below the SMT. The details of both models are included in **Appendix 1**. For the "OSR
764 only" model a C:S ratio of 2:1 at the mudline slowly increases as ^{13}C-depleted carbon is
765 produced. The ESM stations plot near to this model. In the AOM model a C:S ratio of 2.5:1 at
766 the mudline decreases rapidly to an asymptotic value of 1.6:1. The additional flux of DIC from
767 below the SMT prevents the second model from approaching 1:1. Although the height and slope
768 of this model can be changed by altering the fluxes, it shows that CH_4 charged locations with
769 upward migrating DIC must have C:S molar ratios in excess of 1:1. It is possible that this upward
770 flux is a necessary characteristic of all sites with methanogenesis.
771 In summary, from general pore water considerations as well as from comparisons to pore
772 water profiles at other locations, sediments along the ESM continental slope do not contain
773 significant CH_4 in shallow sediment. Implicit in this finding is that sediment sequences along the
774 ESM lack gas hydrate. As models for gas hydrate occurrence in the Arctic (**Figure 1**) correctly
775 predict gas hydrate in several regions (e.g., Kvenvolden and Grantz, 1990; Max and Lowrie,
776 1993; Max and Johnson, 2012), our findings prompt an interesting question: why are predictions
777 so markedly wrong for the ESM?
778
779 *5.7 Explanations*
780 To understand the absence of gas hydrates on the ESM, one needs to consider the
781 generalities of gas hydrate occurrence in marine sediment. There are two basic conditions for gas
782 hydrate on continental slopes (Kvenvolden, 1993; Dickens, 2001). The first is the "potential
783 volume", or the pore space where physiochemical conditions (e.g., temperature, pressure,
784 salinity, sediment porosity) are amenable to gas hydrate formation. As stressed in previous

Biogeosciences Discuss., doi:10.5194/bg-2016-308, 2016
Manuscript under review for journal Biogeosciences
Published: 9 August 2016

works, the ESM, with cold bottom water and a low geothermal gradient, has a relatively large volume of sediment with appropriate gas hydrate stability conditions (Stranne et al., 2016). The second is the "occupancy", or the fraction of sediment pore space with sufficient CH_4 to precipitate gas hydrate. The short answer is that environmental conditions on the ESM are highly conducive for gas hydrate, but there is little CH_4.

It is also important to recognize how diffusive systems operate in marine sediment. Hundreds of pore water profiles have been generated during scientific ocean drilling expeditions, including scores into CH_4 charged sediment sequences. These profiles almost universally show connectivity of pore water chemistry over hundreds of meters (**Figure 2**). This occurs because, given sufficient permeability and time, diffusive fluxes transport species from intervals of high concentration to intervals of low concentration. Hence, unless some impermeable layer exists in the sediment sequence, even CH_4 at depth impacts near seafloor concentrations. Indeed, ODP Leg 164 on the outer Blake Ridge wonderfully shows this phenomenon. The uppermost gas hydrate in sediment in this region probably lies at about 190 mbsf; nonetheless, its presence can be observed in shallow pore water profiles, because the flux of CH_4 from depth drives AOM near the seafloor (Borowski et al., 1999; Dickens, 2001). Assuming that an impermeable layer does not exist in the upper few hundreds of meters of sediment on slopes of the ESM, the lack of gas hydrates and CH_4 suggests either insufficient POC to generate CH_4, or substantial loss of CH_4 over time.

The accumulation of POC on slopes of the ESM may be relatively low over the Plio-Pleistocene, an amount too small to drive methanogenesis. With low POC inputs, other microbial reactions can exhaust the organic matter needed for methanogenesis. This may, in fact, explain why the pore water chemistry suggests that metal-oxide reduction dominates the geochemical

Biogeosciences Discuss., doi:10.5194/bg-2016-308, 2016
Manuscript under review for journal Biogeosciences
Published: 9 August 2016

environment at most stations on the ESM. Without further investigation, we can offer three possibilities as to why this might occur: (1) significant sea-ice concentrations, both at present-day and during past glacial intervals, greatly diminishes primary production within the water column, (2) the extremely broad continental shelf prevents large accumulations of terrestrial organic rich sediment from reaching the slope, or (3) highly variable sediment accumulation, perhaps corresponding to glacial-interglacial oscillations, creates a situation where organic matter can be consumed during intervals of low deposition. In the latter case, large glaciers in the past may have physically removed sediment (and organic matter) from the slope (Jakobsson et al., 2014)

There is also the issue of POC that likely accumulated in the Cretaceous through early Eocene. In theory, organic-rich sediment accumulated around the Arctic during this time, which should have generated CH_4. This CH_4 could either be too deeply buried to migrate into the modern GHSZ or have been lost in the intervening time.

6. Conclusions

Leg 2 of the SWERUS-C3 expedition recovered sediments and pore waters from numerous stations across the ESM continental slope. These stations extend from Wrangel Island to the New Siberian Islands, and give information from a climatically sensitive but highly inaccessible area.

In an effort to understand CH_4 cycling on the ESM continental slope, we generated detailed pore water profiles of multiple dissolved constituents at the stations. The pore water profiles are coherent and interpretable, and give a general view: most stations have low SO_4^{2-} and HCO_3^- fluxes (<9.2 and 6.8 mol/m^2-kyr respectively), a moderate decrease in δ^{13}C-DIC values

Biogeosciences Discuss., doi:10.5194/bg-2016-308, 2016
Manuscript under review for journal Biogeosciences
Published: 9 August 2016

831 with depth (-3.6‰/m average), no dissolved H_2S, moderate rise in HPO_4^{2-} and NH_4
832 concentrations, and slightly decreasing Ca^{2+}, Mg^{2+}, and Sr^{2+} concentrations. Except for one
833 station on the Lomonosov Ridge, metal oxide reduction appears to be the dominant geochemical
834 environment affecting shallow sediment, and there is no evidence for upward diffusing CH_4.
835 These results strongly suggest that gas hydrates do not occur on slopes of the ESM. This directly
836 conflicts with multiple publications, which have assumed large quantities of CH_4 and gas hydrate
837 in the region. It is possible that CH_4 and gas hydrate occur where the Lomonosov Ridge
838 intersects the ESM.
839 The contradiction between models for gas hydrate in the region and actual data may arise
840 for two basic reasons. First, in relatively recent geological times, insufficient POC accumulates
841 along the slope to form CH_4 and gas hydrates; second, CH_4 generated from POC deposited in
842 older geological times is too deeply buried or has been lost.
843
844
845 **Acknowledgments**. The authors would like to thank the SWERUS-C3 Leg 2 crew as well as
846 reviewers.
847

Biogeosciences Discuss., doi:10.5194/bg-2016-308, 2016
Manuscript under review for journal Biogeosciences
Published: 9 August 2016

848 **Table List**

849 **Table 1 -** Rhizon Efficacy

850 **Table 2 -** Rhizon Flow Rates

851 **Table 3 -** QA/QC

852 **Table 4 -** Published and Calculated Fluxes

853 a = Coffin et al., 2013; b = Personal Communication; c = Coffin et al., 2007; d = Coffin et al.,
854 2006; e = Coffin et al., 2008; f = Hamdan et al., 2011 and Coffin et al., 2014; g = Dickens and
855 Snyder, 2009; h= Snyder et al., 2007; i = Mountain et al., 1994; j = Lin et al., 2006; k = Berelson
856 et al., 2005; l = Hensen et al., 2003; m = Dickens, 2001; n = Geprags et al., 2016; o = Claypool et
857 al., 2006; p = Keigwin et al., 1998; q = Berg, 2008; r = Borowski et al., 2000; s = D'Hondt et al.,
858 2002; t = D'Hondt et al., 2004; u = Torres et al., 2009; v = Burns, 1998; w = Kastner et al., 2008;
859 x = Paull et al., 1996; y = Flood et al., 1995; z = Wefer et al., 1998; 1 = Prell et al., 1998; 2 =
860 Takahashi et al., 2011; 3 = Riedel et al., 2006; 4 = Tamaki et al., 1990; 5 = Lyle et al., 1997; 6 =
861 Moore et al., 2001; 7 = Kimura et al., 1997; 8 = Suess et al., 1988; 9 = D'Hondt et al., 2003. ‡ =
862 Calculated from published material.

863 **Table S1 -** All Results

864

865

866 **Figure Captions**

867 **Figure 1.** Generalized Arctic map with background from GeoMapApp
868 (http://www.geomapapp.org; Ryan et al., 2009). Inserted gas hydrate models based on Max and
869 Lowrie, 1993; Max and Johnson, 2012; and Soloviev, 2002.

870

871 **Figure 2.** Idealized pore water concentration profiles for high and low upward methane flux.
872 Discrete data points for sites 722 (Arabian Sea; Seifert and Michaelis, 1991; D'Hondt et al.,
873 2002) and 1230 (offshore Peru; Donohue et al., 2006) are given as reference.

874

875 **Figure 3**. Bathymetric map of the Eurasian Arctic showing the overall cruise track of Leg 2,
876 along with the four transects and coring locations.

877

Biogeosciences Discuss., doi:10.5194/bg-2016-308, 2016
Manuscript under review for journal Biogeosciences
Published: 9 August 2016

878 **Figure 4**. Rhizon sampling of S28 (a) overall core with Rhizon samples inserted and attached to
879 syringes; (b) close-up showing pore water filling syringes.
880
881 **Figure 5.** Measured temperature and pH of Station 33 over 24 hours showing temperature
882 increase and concomitant decrease in pH. Only three pH profiles were collected due to pH meter
883 failure.
884
885 **Figure 6.** Transect 1 results. ACEX results (grey triangles; Backman et al., 2009) and IAPSO
886 standard seawater (black dotted line) shown for comparison.
887
888 **Figure 7.** Transect 2 results. ACEX results (grey triangles; Backman et al., 2009) and IAPSO
889 standard seawater (black dotted line) shown for comparison.
890
891 **Figure 8.** Transect 3 results. ACEX results (grey triangles; Backman et al., 2009) and IAPSO
892 standard seawater (black dotted line) shown for comparison.
893
894 **Figure 9.** Transect 4 results. ACEX results (grey triangles; Backman et al., 2009) and IAPSO
895 standard seawater (black dotted line) shown for comparison.
896
897 **Figure 10.** Lomonosov Ridge Station results. ACEX results (grey triangles; Backman et al.,
898 2009), IAPSO standard seawater (black dotted line), and representative stations from the four
899 transects shown for comparison.
900
901 **Figure 11.** Calcium "error" with sampling time. X-Axis equal to duration of time between core
902 retrieval and rhizon pore water completion.
903
904 **Figure 12.** Relationship of (a) porosity and (b) rhizon extraction rate revealing the (c)
905 exponential correlation in flow rate with porosities commonly observed in piston, gravity, and
906 multicores.
907

Biogeosciences Discuss., doi:10.5194/bg-2016-308, 2016
Manuscript under review for journal Biogeosciences
Published: 9 August 2016

908 **Figure 13.** Relationship of (a) sulfate change (ΔSO_4^{2-}) and carbonate corrected alkalinity change
909 ($\Delta Alk+Ca^{2+}+Mg^{2+}$) following 2:1 ratio; (b) the second order polynomial association of NH_4^+ to
910 Alkalinity; and (c) decreasing $\delta^{13}C$-DIC values with alkalinity increase. Methane charged sites
911 (1230, 1426, and 1427; 1230, Shipboard Scientific Party, 2003; 1426 and 1427, Expedition
912 Scientists, 2014) given for comparison.
913
914 **Figure 14.** C:N:P ratio indirectly shown with $\Delta Alk/\Delta NH_4^+$ and $\Delta Alk/\Delta HPO_4^{2-}$. Several global
915 sites, 994, 995, 997, 1059, 1225, 1230, 1426, 1427, and 1319 (994-997, 1059, Borowski et al.,
916 2000; 1225 and 1230, Shipboard Scientific Party, 2003; 1426 and 1427, Expedition Scientists,
917 2014) given for comparison. Blue marginal distribution curves show global distribution while
918 red gives ESM stations (this project). ESM pore waters have higher C:N and lower C:P than
919 comparative sites.
920
921 **Figure 15.** Bicarbonate (HCO_3^-) and sulfate (SO_4^{2-}) flux exponential relationship with SMT
922 depth for all sites listed in Table 4.
923
924 **Figure 16.** Ratio of carbonate corrected alkalinity change ($\Delta Alk+Ca^{2+}+Mg^{2+}$) and sulfate change
925 (ΔSO_4^{2-}) to the product of DIC and $\delta_{13}C$-DIC value (AT13-2 and KC151, Kastner et al., 2008a;
926 PC02-PC14, Coffin et al., 2008; 994-997, 1059, Borowski et al., 2000; Paull et al., 2000; 1326
927 and 1329, Torres and Kastner, 2009; GC233 and GB425, Hu et al., 2010; D-5 – D-8 and D-F, Hu
928 et al., 2015; C9-C19, Luo et al., 2013; PC-07, Smith and Coffin, 2014; 1230, Shipboard
929 Scientific Party, 2003; 1244 and 1247, Claypool et al., 2006; 1305 and 1306, Party, 2005)
930 including global sites for comparison) showing the paucity of methane charged sites actually
931 reaching 1:1 C:S ratio. Two simple models of OSR and OSR + AOM (following Chatterjee et
932 al., 2011; and Malinverno and Pohlman, 2011); given as dotted lines. When an additional flux of
933 HCO_3^- is added from below the SMT the C:S ratio is unlikely to reach 1:1.
934
935 Error bars are one sigma. ESM plotted pore waters substitute alkalinity for DIC. With the
936 absence of sulfide, DIC and alkalinity should be roughly equivalent in these pore waters. ESM
937 locations use the same symbols as previous figures.

Biogeosciences Discuss., doi:10.5194/bg-2016-308, 2016
Manuscript under review for journal Biogeosciences
Published: 9 August 2016

References:

Aagaard, K., Coachman, L. K., and Carmack, E. C.: On the halocline of the Arctic Ocean, Deep Sea Res., 28, 529-545, 1981.

Aagaard, K. and Carmack, E. C.: The role of sea ice and other fresh water in the Arctic Circulation, J. Geophys. Res., 94, 14485–14498, 1989.

Alekseev, M. N.: Paleogeography and geochronology in the Russian eastern arctic during the second half of the quaternary, Quatern. Int., 41/42, 11–15, 1997.

Alperin, M. J., Reeburgh, W. S., and Whiticar, M. J.: Carbon and hydrogen isotope fractionation resulting from anaerobic methane oxidation, Global Biogeochem. Cy., 2, 279-288, 1988.

Andreassen, K., Hogstad, K., and Berteussen, K. A.: Gas hydrate in the southern Barents Sea indicated by a shallow seismic anomaly, First Break, 8, 235–245, 1990.

Andreev, A. A., Grosse, G., Schirrmeister, L., Kuznetsova, T. V., Kuzmina, S. A., Bobrov, A. A., Tarasov, P. E., Novenko, E., Yu., Meyer, H., Derevyagin, A., Yu., Kienast, F., Bryantseva, A., and Kunitsky, V. V.: Weichselian and Holocene palaeoenvironmental history of the Bol'shoy Lyakhovsky Island, New Siberian Archipelago, Arctic Siberia. Boreas 38, 72–110, 2009.

Archer, D. E.: Methane hydrate stability and anthropogenic climate change, Biogeosciences, 4, 993-1057, 2007.

Archer, D.: A model of the methane cycle, permafrost, and hydrology of the Siberian continental margin, Biogeosciences, 12 (10), 2953–2974, 2015.

Augstein, E.: Die Expedition ARCTIC'96 mit FS" Polarstern"(ARK XII) mit der Arctic Climate System Study (ACSYS); The expedition ARCTIC'96 of RV" Polarstern"(ARK XII) with the Arctic Climate System Study (ACSYS). Berichte zur Polarforschung (Reports on Polar Research), 234, 1997.

Biogeosciences Discuss., doi:10.5194/bg-2016-308, 2016
Manuscript under review for journal Biogeosciences
Published: 9 August 2016

962 Backman, J., and Moran, K.: Expanding the Cenozoic paleoceanographic record in the Central
963 Arctic Ocean: IODP Expedition 302 Synthesis: Central European Journal of Geosciences,
964 1, 2, 157-175, 2009.
965 Bakhmutov, V., Whitledge, T., Wood, K. and Ostrovskiy, A.: Report on the execution of marine
966 research in the Bering Strait, East Siberian and the Chukchi Sea by the Russian-American
967 Expedition under the program of" RUSALCA" during the period from 23 August through
968 30 September, 2009.
969 Barnes, R. O. and Goldberg, E. D.: Methane production and consumption in anoxic marine
970 sediments, Geol. 4, 297–300, 1976.
971 Beaudoin, Y. C., Waite, W., Boswell, R., and Dallimore, S. R.: Frozen Heat: A UNEP Global
972 Outlook on Methane Gas Hydrates. Volume 1. UN. Environ. Programme, GRID-Arendal,
973 2014
974 Berelson, W. M., Prokopenko, M., Sansone, F. J., Graham, A. W., McManus, J. and Bernhard, J.
975 M.: Anaerobic diagenesis of silica and carbon in continental margin sediments: discrete
976 zones of TCO 2 production. Geochimica et cosmochimica acta, 69 (19), 4611-4629,
977 2005.
978 Berg, P., Risgaard-Petersen, N., and Rysgaard, S.: Interpretation of measured concentration
979 profiles in sediment pore water, Limnol. Oceanogr., 43, 1500-1510, 1998.
980 Berg, R.D.: Diffusional methane fluxes within continental margin sediments and depositional
981 constraints on formation factor estimates, ProQuest, 2008.
982 Berner, R. A.: Diagenetic models of dissolved species in the interstitial waters of compacting
983 sediments, Am. J. Sci., 275, 88–96, 1975.

Biogeosciences Discuss., doi:10.5194/bg-2016-308, 2016
Manuscript under review for journal Biogeosciences
Published: 9 August 2016

984 Berner, R. A.: Stoichiometric models for nutrient regeneration m anoxic sediment?, Limnology,
985 22, 781-786, 1977
986 Berner, R. A.: Early Diagenesis: A Theoretical Approach, Princeton University Press, Princeton,
987 N. J., 1980.
988 Bhatnagar, G., Chatterjee, S., Chapman, W. G., Dugan, B., Dickens, G. R., and Hirasaki G. J.:
989 Analytical theory relating the depth of the sulfate-methane transition to gas hydrate
990 distribution and saturation, Geochem. Geophy. Geosy., 12, 1-21, 2011.
991 Biastoch, A., Treude, T., Ruepke, L. H., Riebesell, U., Roth, C., Burwicz, E. B., Park, W., Latif,
992 M., Boening, C. W., Madec, G., and Wallmann, K.: Rising Arctic Ocean temperatures
993 cause gas hydrate destabilization and ocean acidification, Geophys. Res. Lett., 38, 1-5,
994 2011.
995 Boetius, A., Ravenschlag, K., Schubert, C. J., Rickert, D., Widdel, F., Gieseke, A., Amann, R.,
996 Jørgensen, B. B., Witte, U. and Pfannkuche, O.: A marine microbial consortium
997 apparently mediating anaerobic oxidation of methane, Nature, 407, 623-626, 2000.
998 Borowski, W. S., Paull, C. K., and Ussler III, W.: Marine porewater sulfate profiles indicate in
999 situ methane flux from underlying gas hydrate, Geol. 24, 655– 658, 1996.
1000 Borowski, W. S., Paull, C. K., and Ussler W. III: Global and local variations of interstitial sulfate
1001 gradients in deepwater, continental margin sediments: Sensitivity to underlying methane
1002 and gas hydrates, Mar. Geol., 159, 131–154, 1999.
1003 Borowski, W. S., Hoehler, T. M., Alperin, M. J., Rodriguez, N. M. and Paull, C.K.: Significance
1004 of anaerobic methane oxidation in methane-rich sediments overlying the Blake Ridge gas
1005 hydrates. In Proceedings of the ocean drilling program, scientific results (Vol. 164, pp.
1006 87-99, 2000).

1007 Borowski, W. S., Cagatay, N., Ternois, Y., and Paull, C. K.: Data Report: carbon isotopic
1008 composition of dissolved CO2, CO2 gas, and methane, Blake –Bahama Ridge and
1009 Northeast Bermuda Rise, ODP Leg 172, In: Keigwin, L. D., Rio, D., Acton, G. D.,
1010 Arnold, E. (Eds.), Proceedings of the ODP. Scientific Results (College Station, TX), vol.
1011 172, 1–16, 2001.
1012 Boudreau, B. P. and Westrich, J. T.: The dependence of bacterial sulfate reduction on sulfate
1013 concentration in marine sediments, Geochimica Cosmochimica Acta, 48, 2503–2516,
1014 1984.
1015 Buffett, B. and Archer, D.: Global inventory of methane clathrate: sensitivity to changes in the
1016 deep ocean, Earth Planet. Sc. Lett., 227, 185–199, 2004.
1017 Burns, S.J.: Carbon isotopic evidence for coupled sulfate reduction-methane oxidation in
1018 Amazon Fan sediments. Geochimica et Cosmochimica Acta, 62(5), 797-804, 1998.
1019 Carcione, J. M. and Tinivella, U.: Bottom-simulation reflectors: Seismic velocities and AVO
1020 effects, Geophysics, 65, 54–67, 2000.
1021 Chatterjee, S., Dickens, G. R., Bhatnagar, G., Chapman, W. G., Dugan, B., Snyder, G. T., and
1022 Hirasaki, G. J.: Pore water sulfate, alkalinity, and carbon isotope profiles in shallow
1023 sediment above marine gas hydrate systems: A numerical modeling perspective, J.
1024 Geophys. Res-Sol. Ea., 116, 1-25, 2011.
1025 Chand, S., Mienert, J., Andreassen, K., Knies, J., Plassen, L., and Fotland, B.: Gas hydrate
1026 stability zone modelling in areas of salt tectonics and pockmarks of the Barents Sea
1027 suggests an active hydrocarbon venting system, Mar. Petrol. Geol., 25, 625–636, 2008.
1028 Clark, D. L.: Early history of the Arctic Ocean, Paleoceanography, 3, 539-550, 1988.

1029 Claypool, G. E. and Kvenvolden, K. A.: Methane and other hydrocarbon gases in marine
1030 sediment, Annu. Rev. Earth Pl. Sc., 11, 299-327, 1983.
1031 Claypool, G. E., Milkov, A. V., Lee, Y. J., Torres, M. E., Borowski, W.S., and Tomaru, H.:
1032 Microbial Methane Generation and Gas Transport in Shallow Sediments of an
1033 Accretionary Complex, Southern Hydrate Ridge (ODP Leg 204), Offshore Oregon USA,
1034 In: Trehu, A.M., Bohrmann, G., Torres, M.E., Colwell, F.S. (Eds.), In Proceedings of the
1035 ODP, Scientific Results. Ocean Drilling Program, College Station, Texas, 2006.
1036 Cline, J. D.: Spectrophotometric determination of hydrogen sulfide in natural waters, Limnol.
1037 Oceanogr., 14, 454-458, 1969.
1038 Coffin, R. B., Pohlman, J. W., Gardner, J., Downer, R., Wood, W., Hamdan, L., Walker, S.,
1039 Plummer, R., Gettrust, J., and Diaz, J.: Methane hydrate exploration on the mid Chilean
1040 coast: a geochemical and geophysical survey, J. Petrol. Sci. Eng., 56, 32-41, 2007.
1041 Coffin, R., Hamdan, L., Pohlman, J., Wood, W., Pecher, I., Henrys, S., Greinert, J., and Faure,
1042 K.: Geochemical characterization of concentrated gas hydrate deposits on the Hikurangi
1043 Margin, New Zealand. Preliminary Geochemical Cruise Report. NRL/MR/ 6110-07,
1044 2007.
1045 Coffin, R. B., Hamdan, L. J., Plummer, R., Smith, J., Gardner, J., Hagen, R., and Wood, W.:
1046 Analysis of Methane and Sulfate Flux in Methane-charged Sediments from the
1047 Mississippi Canyon, Gulf of Mexico, Mar. Petrol. Geol., 25, 977–987, 2008.
1048 Coffin, R. B., Plummer, R. B., Yoza, B., Larsen, R. K., Millholland, L. C., and Montgomery, M.
1049 T.: Spatial variation in shallow sediment methane sources and cycling on the Alaskan
1050 Beaufort Sea Shelf/Slope, Mar. Petrol. Geol., 45, 186-197, 2013.

1051 Coffin, R. B., Hamdan, L. J., Smith, J. P., Rose, P. S., Plummer, R. E., Yoza, B., Pecher, I. and
1052 Montgomery, M.T.: Contribution of vertical methane flux to shallow sediment carbon
1053 pools across Porangahau ridge, New Zealand. Energies, 7 (8), 5332-5356, 2014.
1054 Collett, T.S.: Energy resource potential of natural gas hydrates, AAPG Bull., 86, 1971–1992,
1055 2002.
1056 Collett, T. S., Lee, M. W., Agena, W. F., Miller, J. J., Lewis, K. A., Zyrianova, M. V., Boswell,
1057 R., and Inks, T. L.: Permafrost associated natural gas hydrate occurrences on the Alaska
1058 North Slope, Mar. Petrol. Geol., 28, 279-294, 2010.
1059 D'Hondt, S., Rutherford, S., and Spivack, A.J.: Metabolic activity of subsurface life in deep-sea
1060 sediments, Science, 295, 2067-2070, 2002.
1061 D'Hondt, S. L., Jørgensen, B. B., Miller, D. J., and Shipboard Scientific Pary: Proceedings of the
1062 Ocean Drilling Program, Initial Reports Volume 201, 2003.
1063 D'Hondt, S., Jørgensen, B. B., Miller, D. J., Batzke, A., Blake, R., Cragg, B. A., Cypionka, H.,
1064 Dickens, G. R., Ferdelman, T., Hinrichs, K. U. and Holm, N.G.: Distributions of
1065 microbial activities in deep subseafloor sediments. Science, 306 (5705), 2216-2221,
1066 2004.
1067 Danyushevskaya, A., Yashin, D. S., and Kirillow, O. V.: Geochemical patterns of distribution of
1068 organic carbon in the bottom sediments of Arctic seas, Oceanology, 20, 183-188, 1980.
1069 Darby, D. A., Naidu, A. S., Mowatt, T. C., and Jones, G.: Sediment composition and
1070 sedimentary processes in the Arctic Ocean. In: Y. Herman (Editor), The Arctic Seas:
1071 Climatology, Oceanography, Geology and Biology, Van Nostrand Reinhold, New York,
1072 657-720, 1989.

1073 De Lange, G. J., Cranston, R. E., Hydes, D. H. and Boust, D.: Extraction of pore water from
1074 marine sediments: A review of possible artifacts with pertinent examples from the North
1075 Atlantic. Mar. Geol., 109, 53-76, 1992.
1076 Dehairs, F., Chesselet, R., and Jedwab, J.: Discrete suspended particles of barite and the barium
1077 cycle in the ocean, Earth Planet. Sci. Lett., 49, 528–550, 1980.
1078 Devol, A. H.: Are high rates of sulphate reduction associated with anaerobic oxidation of
1079 methane?, Nature, 291, 407-408, 1981.
1080 Dickens, G. R., Paull, C. K. and Wallace, P.: Direct measurement of in situ methane quantities in
1081 a large gas hydrate reservoir. Nature, 385, 426-428, 1997.
1082 Dickens, G. R.: Sulfate profiles and barium fronts in sediment on the Blake Ridge. Present and
1083 past methane fluxes through a large gas hydrate reservoir, Geochim. Cosmochim. Ac.,
1084 65, 529-543, 2001.
1085 Dickens, G. R.: Rhizon sampling of pore waters on scientific drilling expeditions: an example
1086 from the IODP Expedition 302, Arctic Coring Expedition (ACEX). Sci. Drill 4, 22–25,
1087 2007.
1088 Dickens, G.R. and Snyder, G.T.: Interpreting upward methane flux from marine pore water
1089 profiles, In: Fire in the Ice, NETL Methane Hydrate Newsletter 9 (1), 7-10, 2009.
1090 Domenico, P.A. and Schwartz, F.W.: Physical and chemical hydrogeology, (Vol. 44), New
1091 York: Wiley, 1998.
1092 D'Hondt, S., Rutherford, S., and Spivack, A. J.: Metabolic activity of subsurface life in deep-sea
1093 sediments, Science, 295, 2067–2070, 2002.
1094 Dmitrenko, I. A., Polyakov, I. V., Kirillov, S. A., Timokhov, L. A., Frolov, I. E., Sokolov, V. T.,
1095 Simmons, H. L., Ivanov, V. V., and Walsh, D.: Toward a warmer Arctic Ocean:

spreading of the early 21st century Atlantic Water warm anomaly along the Eurasian Basin margins, J. Geophys. Res-Oceans 113, 1-13, 2008.

Dmitrenko, I. A., Bauch, D., Kirillov, S. A., Koldunov, N., Minnett, P. J., Ivanov, V. V., Hölemann, J. A., and Timokhov, L. A.: Barents Sea upstream events impact the properties of Atlantic water inflow into the Arctic Ocean: Evidence from 2005 to 2006 downstream observations, Deep-Sea Research I, 56, 513–527, 2009

Donohue, C. M., Snyder, G. T., and Dickens, G. R.: Data report: major cation concentrations of interstitial waters collected from deep sediments of Eastern Equatorial Pacific and Peru Margin (ODP Leg 201), Proceedings of ODP, Scientific Results, 201, Ocean Drilling Program, College Station, TX, 2006.

Dymond, J., Suess, E., and Lyle, M.: Barium in deep-sea sediment: A geochemical proxy for paleoproductivity, Paleoceanography 7, 163–181, 1992.

Elliott, S., Maltrud, M., Reagan, M., Moridis, G., and Cameron-Smith P.: Marine methane cycle simulations for the period of early global warming, J. Geophys. Res-Biogeo., 116, 1-13, 2011.

Engen, Ø., Faleide, J. I., and Dyreng, T. K.: Opening of the Fram Strait gateway: A review of plate tectonic constraints: Tectonophysics, 450, 1-69, 2008.

Expedition 346 Scientists: Asian Monsoon: onset and evolution of millennial-scale variability of Asian monsoon and its possible relation with Himalaya and Tibetan Plateau uplift, IODP Preliminary Report, 346, 2014.

Eiken, O. and Hinz, K.: Contourites in the Fram Strait, Sediment Geol., 82, 15–32, 1993.

Biogeosciences Discuss., doi:10.5194/bg-2016-308, 2016
Manuscript under review for journal Biogeosciences
Published: 9 August 2016

1117 Ferré, B., Mienert, J., and Feseker, T.: Ocean temperature variability for the past 60 years on the
1118 Norwegian-Svalbard margin influences gas hydrate stability on human time scales, J.
1119 Geophys. Res., 117, 1-14, 2012.
1120 Flood, R. D., Piper, D. J. W., Klaus, A., and Scientific Research Party: Proceedings of the Ocean
1121 Drilling Program, Initial Reports, 155: College Station, TX (Ocean Drilling Program),
1122 1995.
1123 Froelich, P., Klinkhammer, G. P., Bender, M. A. A., Luedtke, N. A., Heath, G. R., Cullen, D.,
1124 Dauphin, P., Hammond, D., Hartman, B., and Maynard, V.: Early oxidation of organic
1125 matter in pelagic sediments of the eastern equatorial Atlantic: suboxic diagenesis,
1126 Geochim. Cosmochim. Ac., 43, 1075-1090, 1979.
1127 Gao, H., Schreiber, F., Collins, G., Jensen, M. M., Kostka, J. E., Lavik, G., de Beer, D., Zhou, H.
1128 Y., and Kuypers, M. M.: Aerobic denitrification in permeable Wadden Sea sediments,
1129 The ISME J., 4, 417-426, 2010.
1130 Geprägs, P., Torres, M. E., Mau, S., Kasten, S., Römer, M., and Bohrmann, G.: Carbon cycling
1131 fed by methane seepage at the shallow Cumberland Bay, South Georgia, sub-Antarctic,
1132 Geochem. Geophy. Geosy., 17, 1401-1418, 2016.
1133 Gieskes, J. M. and Rogers, W. C.: Alkalinity determination in interstitial waters of marine
1134 sediments, J. Sediment. Res., 43(1), 272-277, 1973.
1135 Gieskes J. M.: The alkalinity-total carbon dioxide system in seawater, In The Sea, vol. 5 (ed. E.
1136 D. Goldberg). John Wiley and Sons, New York, 123–151, 1974.
1137 Gieskes, J. M., Gamo, T., and Brumsack, H.: Chemical methods for interstitial water analysis
1138 aboard JOIDES Resolution, 1991.

Biogeosciences Discuss., doi:10.5194/bg-2016-308, 2016
Manuscript under review for journal Biogeosciences
Published: 9 August 2016

1139 Gingele, F. and Dahmke, A.: Discrete barite particles and barium as tracers of paleoproductivity
1140 in South Atlantic sediments, Paleoceanography, 9, 151–168, 1994.
1141 Giustiniani, M., Tinivella, U., Jakobosson, M., and Rebesco, M.: Arctic Ocean gas hydrate
1142 stability in a changing climate, J. Geol. Res., 1-10, 2013.
1143 Goldhaber, M.: Kinetic Models of Sulfur Diagenesis in Recent Marine Sediments, In
1144 Transactions-AGU, 55, 696-697, 1974.
1145 Grantz, A., Boucher, G., and Whitney, O. T.: Possible solid gas hydrate and natural gas deposits
1146 beneath the continental slope of the Beaufort Sea, U.S. Geological Survey Circulation
1147 Number 733, 1976.
1148 Grantz, A., Mann, D. M., and May, S. D.: Tracklines of multichannel seismic-reflection data
1149 collected by the U.S. Geological Survey in the Beaufort and Chukchi Seas in 1977 for
1150 which profiles and stack tapes are available, U.S. Geological Survey Open-File Report
1151 1982, 82-735, 1982.
1152 Greinert, J., Bohrmann, G., and Suess, E.: Gas hydrate-associated carbonates and methane-
1153 venting at Hydrate Ridge: classification, distribution, and origin of authigenic lithologies,
1154 Natural gas hydrates: Occurrence, distribution, and detection, 99-113, 2001.
1155 Gualtieri, L., Vartanyan, S., Brigham-Grette, J., and Anderson, P. M.: Evidence for an ice-free
1156 Wrangel Island, Northeast Siberia during the Last Glacial Maximum, Boreas 34, 264–
1157 273, 2005.
1158 Gusev, E., Anikina, N., Andreeva, I., Bondarenko, S., Derevyanko, L., Iosifidi, A., Klyuvitkina,
1159 T., Litvinenko, I., Petrova, V., Polyakova, E., Popov, V., and Stepanova, A.: Stratigraphy
1160 of Late Cenozoic sediments of the western Chukchi Sea: New results of shallow drilling
1161 and seismic reflection profiling, Global Planet. Change, 68, 115–131, 2009.

Biogeosciences Discuss., doi:10.5194/bg-2016-308, 2016
Manuscript under review for journal Biogeosciences
Published: 9 August 2016

1162 Haacke, R. R., Westbrook, G. K., and Riley, M.: Controls on the formation and stability of gas
1163 hydrate-related bottom-simulating reflectors (BSRs): a case study from the west Svalbard
1164 continental slope, J. Geophys. Res., 113, 1-17, 2008.
1165 Hamdan, L. J., Gillevet, P. M., Pohlman, J. W., Sikaroodi, M., Greinert, J., and Coffin, R.B.:
1166 Diversity and biogeochemical structuring of bacterial communities across the Porangahau
1167 ridge accretionary prism, New Zealand, FEMS Microbiol. Ecol., 77, 518-532, 2011.
1168 Haraldsson, C., Anderson, L. G., Hassellöv, M., Hulth, S., and Olsson, K.: Rapid, high-precision
1169 potentiometric titration of alkalinity in ocean and sediment pore waters, Deep Sea
1170 Research Part I: Oceanographic Research Papers, 44, 2031-2044, 1997.
1171 Hart, P. E., Pohlman, J. W., Lorenson, T. D., and Edwards, B. D.: Beaufort Sea Deep-water gas
1172 hydrate recovery from a seafloor mound in a region of widespread BSR occurence, in
1173 Proceedings of the 7th International Conference on Gas Hydrates (ICGH 2011),
1174 Edinburgh, Scotland, 2011.
1175 Hensen, C., Zabel, M., Pfiefer, K., Schwenk, T., Kasten, S., Riedinger, N., Schulz, H. D.,
1176 Boetius, A.: Control of sulfate porewater profiles by sedimentary events and the
1177 significance of anaerobic oxidation of methane for the burial of sulfur in marine
1178 sediments, Geochimica Cosmochimica Acta 67, 2631-2647, 2003.
1179 Holbrook, W. S., Hoskins, H., Wood, W. T., Stephen, R. A., and Lizarralde, D.: Methane hydrate
1180 and free gas on the Blake ridge from vertical seismic profiling, Science, 273, 1840–1843,
1181 1996.
1182 Holmes, R. M., McClelland, J. W., Peterson, B. J., Shiklomanov, I. A., Shiklomanov, A. I.,
1183 Zhulidov, A. V., Gordeev, V. V., and Bobrovitskaya, N. N.: A circumpolar perspective
1184 on fluvial sediment flux to the Arctic Ocean, Global Biogeochem. Cy., 16, 1-14, 2002.

1185 Holler, T., Wegener, G., Knittel, K., Boetius, A., Brunner, B., Kuypers, M. M., and Widdel, F.:
1186 Substantial 13C/12C and D/H fractionation during anaerobic oxidation of methane by
1187 marine consortia enriched in vitro, Environ. Microbiol. Rep., 1, 370-376, 2009.
1188 Hovland, M. and Svensen, H.: Submarine pingoes: Indicators of shallow gas hydrates in a
1189 pockmark at Nyegga, Norwegian Sea, Mar. Geol., 228, 15–23, 2006.
1190 Hu, X., Cai, W. -J, Wang, Y., Luo, S., and Guo X.: Pore-water geochemistry of two contrasting
1191 brine-charged seep stations in the northern Gulf of Mexico continental slope, Mar.
1192 Geochem., 118, 99–107, 2010.
1193 Hu, Y., Feng, D., Liang, Q., Xia, Z., Chen, L., and Chen, D.: Impact of anaerobic oxidation of
1194 methane on the geochemical cycle of redox-sensitive elements at cold-seep stations of the
1195 northern South China Sea. Deep Sea Research Part II: Topical Studies in Oceanography,
1196 2015.
1197 Hustoft, S., Bünz, S., Mienert, J., and Chand, S.: Gas hydrate reservoir and active methane-
1198 venting province in sediments on <20Ma young oceanic crust in the Fram Strait, offshore
1199 NW-Svalbard, Earth Planet. Sc. Lett., 284, 12-24, 2009.
1200 Hyndman, R. D. and Dallimore, S. R.: Natural gas hydrates studies, Canada Recorder, 26, 11–20,
1201 2001.
1202 Jakobsson, M.: Hypsometry and volume of the Arctic Ocean and its constituent seas:
1203 Geochemistry, Geophysics, Geosystems, 3, 5, 1-18, 2002
1204 Jakobsson, M., Grantz, A., Kristoffersen, Y., and Macnab, R.: Physiographic provinces of the
1205 Arctic Ocean seafloor, GSA Bull., 115, 1443-1455, 2003.
1206 Jakobsson, M., Backman, J., Rudels, B., Nycander, J., Frank, M., Mayer, L., Jokat, W.,
1207 Sangiorgi, F., O'Regan, M., Brinkhuis, H., King, J., and Moran, K.: The early Miocene

1208 Onset of a Ventilated Circulation Regime in the Arctic Ocean: Nature, 447, 21, 986-990,
1209 2007.
1210 Jakobsson, M., Polyak, L., Edwards, M., Kleman, J., and Coakley, B.: Glacial geomorphology of
1211 the Central Arctic Ocean: the Chukchi Borderland and the Lomonosov Ridge, Earth Surf.
1212 Proc. Land., 33, 526-545, 2008.
1213 Jakobsson, M., Andreassen, K., Bjarnadóttir, L. R., Dove, D., Dowdeswell, J. A., England, J. H.,
1214 Funder, S., Hogan, K., Ingólfsson, Ó., Jennings, A., Krog-Larsen, N., Kirchner, N.,
1215 Landvik, J. Y., Mayer, L., Möller, P., Niessen, F., Nilsson, J., O'Regan, M., Polyak, L.,
1216 Nørgaard-Pedersen, N., and Stein, R.: Arctic Ocean glacial history, Quaternary Sci. Rev.,
1217 92, 40-67, 2014.
1218 Jørgensen, B. B., Bang, M., and Blackburn, T. H.: Anaerobic mineralization in marine sediments
1219 from the Baltic Sea-North Sea transition, Mar. Ecol. Progress Series, 59, 39-54, 1990.
1220 Jørgensen, B. B., Weber, A. and Zopfi, J.: Sulfate reduction and anaerobic methane oxidation in
1221 Black Sea sediments. Deep Sea Research Part I: Oceanographic Research Papers, 48 (9),
1222 2097-2120, 2001.
1223 Jørgensen, B. B., Böttcher, M. E., Lüschen, H., Neretin, L. N., and Volkov, I. I.: Anaerobic
1224 methane oxidation and the deep H2S sink generate isotopically heavy sulfides in Black
1225 Sea sediments, Geochim. Cosmochim. Ac., 68, 2095–2118, 2004.
1226 Jørgensen, B. B. and Parkes, R. J.: Role of sulfate reduction and methane production by organic
1227 carbon degradation in eutrophic fjord sediments (Limfjorden, Denmark), Limnol.
1228 Oceanogr, 55, 1338-1352, 2010.

Biogeosciences Discuss., doi:10.5194/bg-2016-308, 2016
Manuscript under review for journal Biogeosciences
Published: 9 August 2016

1229 Jokat, W.: The expedition of the Research Vessel" Polarstern" to the Arctic in 2009 (ARK-
1230 XXIV/3). Berichte zur Polar-und Meeresforschung (Reports on Polar and Marine
1231 Research), 615, 2010.
1232 Jokat, W. and Ickrath, M.: Structure of ridges and basins off East Siberia along 81° N, Arctic
1233 Ocean, Mar. Petrol. Geol., 64, 222-232, 2015.
1234 Joye, S. B., Boetius, A., Orcutt, B. N., Montoya, J. P., Schulz, H. N., Erickson, M. J. and Lugo,
1235 S.K.: The anaerobic oxidation of methane and sulfate reduction in sediments from Gulf
1236 of Mexico cold seeps. Chemical Geology, 205 (3), 219-238, 2004.
1237 Jenkyns, H. C., Forster, A., Schouten, S., and Sinninghe Damsté, J. S.: High temperatures in the
1238 Late Cretaceous Arctic Ocean, Nature, 432, 888–892, 2004.
1239 Judge, A. S.: Natural gas hydrates in Canada, In: M.H. French (Editor), Proceedings of the
1240 Fourth Canadian Permafrost Conference 1981, Roger J.E. Brown Memorial Volume,
1241 National Research Council of Canada, Ottawa, Ont., 320-328, 1982.
1242 Kastner, M., Claypool, G., and Robertson, G.: Geochemical constraints on the origin of the pore
1243 fluids and gas hydrate distribution at Atwater Valley and Keathley Canyon, northern Gulf
1244 of Mexico, Mar. Petr. Geol., 25, 860–872, 2008a.
1245 Kastner, M., Torres, M., Solomon, E., and Spivack, A. J.: Marine pore fluid profiles of dissolved
1246 sulfate; do they reflect in situ methane fluxes?, In: Fire in the Ice, NETL Methane
1247 Hydrate Newsletter, Summer, 2008b.
1248 Keigwin, L. D., Rio, D., Acton, G. D., and Shipboard Scientific Party: Proceedings of the Ocean
1249 Drilling Program, Initial Reports, 172: College Station, TX (Ocean Drilling Program),
1250 1998.

1251 Kimura, G., Silver, E. A., Blum, P., Shipboard Scientific Party: Proceedings of the Ocean
1252 Drilling Program, Initial Reports, Vol. 170, 1997.
1253 Klauda, J. B. and Sandler, S. I.: Global distribution of methane hydrate in ocean sediment,
1254 Energy Fuel, 19, 469–78, 2005.
1255 Klump, J. V. and Martens, C. S.: Biogeochemical cycling in an organic rich coastal marine
1256 basin—II. Nutrient sediment-water exchange processes, Geochim. Cosmochim. Ac., 45,
1257 101-121, 1981.
1258 Kvenvolden, K. A., and Grantz, A.: Gas hydrates in the Arctic Ocean region, in The Arctic
1259 Ocean Region, Geology of North America, Geol. Soc. of Am., Boulder, Colo., 539-549,
1260 1990.
1261 Kvenvolden, K. A.: Gas hydrates: Geological perspective and global change, Rev. Geophys., 31,
1262 173–187, 1993.
1263 Kvenvolden, K. A. and Lorenson, T. D.: The global occurrence of natural gas hydrate. In: Paull,
1264 C. K., Dillon, W. P. (Eds.), Natural Gas Hydrates: Occurrence, Distribution, and
1265 Detection, AGU Geophy. Monograph Ser., 124, 3–18, 2001.
1266 Laberg, J. S. and Andreassen, K.: Gas hydrate and free gas indications within the Cenozoic
1267 succession of the Bojornya Basin, western Barents Sea, Mar. Petrol. Geol., 13, 921-940,
1268 1996.
1269 Laberg, J. S., Andreassen, K., and Knutsen, S. M.: Inferred gas hydrate on the Barents Sea shelf
1270 a model for its formation and a volume estimate, Geo-Mar. Lett., 18, 26–33, 1998.
1271 Lerman, A.: Migrational processes and chemical reactions in Sulfate profiles and barium fronts
1272 in sediment 539 interstitial waters, In The Sea, Volume VI (ed. E. D. Goldberg), Wiley,
1273 New York, 695-738, 1977.

Biogeosciences Discuss., doi:10.5194/bg-2016-308, 2016
Manuscript under review for journal Biogeosciences
Published: 9 August 2016

1274 Li, Y-H. and Gregory, S.: Diffusion of ions in sea sediments. Geochim. Cosmochim. Ac., 38,
1275 703-714, 1974.
1276 Lin, S., Hsieh, W. C., Lim, Y. C., Yang, T. F., Liu, C. S., and Wang, Y.: Methane migration and
1277 its influence on sulfate reduction in the Good Weather Ridge region, South China Sea
1278 continental margin sediments, Terr. Atmos. Ocean. Sci., 17, 883-902, 2006.
1279 Lorenson, T. D. and Kvenvolden, K. A.: Methane in coastal seawater, sea ice, and bottom
1280 sediments, Beaufort Sea, Alaska, USGS Open-File Report 95–70, 1995.
1281 Løvø, V., Elverhøi, A., Antonsen, P., Solheim, A., Butenko, G., Gregersen, O., and Liestøl O.:
1282 Submarine permafrost and gas hydrates in the northern Barents Sea, Norsk Polarinstitutt
1283 Rapportserie, 56, 1-171, 1990.
1284 Luff, R. and Wallmann, K.: Fluid flow, methane fluxes, carbonate precipitation and
1285 biogeochemical turnover in gas hydrate-bearing sediments at hydrate ridge, Cascadia
1286 margin: numerical modeling and mass balances, Geochim. Cosmochim. Ac., 67, 3403–
1287 3421, 2003.
1288 Luo, M., Chen, L., Wang, S., Yan, W., Wang, H., and Chen, D.: Pockmark activity inferred from
1289 pore water geochemistry in shallow sediments of the pockmark field in southwestern
1290 Xisha Uplift, northwestern South China Sea, Mar. Pet. Geol., 2013, 48, 247–259, 2013.
1291 Lyle, M., Koizumi, I., Richter, C., and Shipboard Scientific Party: Proceedings of the Ocean
1292 Drilling Program, Initial Reports, Vol. 167, 1997.
1293 MacKay, M. E., Jarrard, R. D., Westbrook, G. K., Hyndman, R. D., and Shipboard Scientific
1294 Party: Origin of bottom-simulating reflectors: geophysical evidence from the Cascadia
1295 accretionary prism, Geol., 22, 459–462, 1994.

Biogeosciences Discuss., doi:10.5194/bg-2016-308, 2016
Manuscript under review for journal Biogeosciences
Published: 9 August 2016

1296 Majorowicz, J. A. and Osadetz, K. G.: Gas hydrate distribution and volume in Canada. AAPG
1297 bulletin, 85 (7), 1211-1230, 2001.
1298 Makogon, Y. F.: Natural gas hydrates–A promising source of energy, J. Nat. Gas Sc. Eng., 2, 49-
1299 59, 2010.
1300 Malinverno, A. and Pohlman, J. W.: Modeling sulfate reduction in methane hydrate-bearing
1301 continental margin sediments: does a sulfate-methane transition require anaerobic
1302 oxidation of methane, Geochem. Geophy. Geosy., 12, 1-18, 2011.
1303 Max, M. D. and Lowrie, A.: Natural gas hydrates: Arctic and Nordic Sea potential. Arctic
1304 geology and petroleum potential, proceedings of the Norwegian Petroleum Society
1305 conference, 15-17 August 1990, Tromsø, Norway. No. 2. Elsevier Science Ltd., 1993.
1306 Max, M. D. and Johnson, A. H.: Natural Gas Hydrate (NGH) Arctic Ocean potential prospects
1307 and resource base, OTC Arctic Technology Conference, 27-53, 2012.
1308 McGuire, A. D., Anderson, L. G., Christensen, T. R., Dallimore, S., Guo, L. D., Hayes, D. J.,
1309 Heimann, M., Lorenson, D. D., MacDonald, R. W., and Roulet, N.: Sensitivity of the
1310 carbon cycle in the Arctic to climate change, Ecol. Monogr., 79, 523–555, 2009.
1311 Miles, P. R.: Potential distribution of methane hydrate beneath the European continental margins,
1312 Geophys. Res. Lett., 22, 3179-3182, 1995.
1313 Miller, M. D., Adkins, J. F., and Hodell, D. A.: Rhizon sampler alteration of deep ocean
1314 sediment interstitial water samples, as indicated by chloride concentration and oxygen
1315 and hydrogen isotopes, Geochem. Geophy. Geosy., 15, 2401-2413, 2014.
1316 Moore, G. F., Taira, A., and Klaus, A., and Shipboard Scientific Party: Proceedings of the Ocean
1317 Drilling Program, Initial Reports Volume 190, 2001.

Biogeosciences Discuss., doi:10.5194/bg-2016-308, 2016
Manuscript under review for journal Biogeosciences
Published: 9 August 2016

1318 Moran, K., Backman, J., Brinkhuis, H., Clemens, S. C., Cronin, T., Dickens, G. R., Eynaud, F.,
1319 Gattacceca, J., Jakobsson, M., Jordan, R.W., and Kaminski, M.: The Cenozoic
1320 palaeoenvironment of the arctic ocean, Nature, 441, 601-605, 2006.
1321 Mountain, G. S., Miller, K. G., Blum, P., and Shipboard Scientific Party: Proc. ODP, Initial
1322 Reports, 150: College Station, TX (Ocean Drilling Program), 1994.
1323 Murray, R. W., Miller, D. J., and Kryc, K. A.: Analysis of major and trace elements in rocks,
1324 sediments, and interstitial waters by inductively coupled plasma–atomic emission
1325 spectrometry (ICP-AES), ODP Technical Note 29, 2000.
1326 Naidu, A. S., Cooper, L. W., Finney, B. P., Macdonald, R. W., Alexander, C., and Semiletov, I.
1327 P.: Organic carbon isotope ratios (δ13C) of Arctic Amerasian continental shelf sediments,
1328 Int. J. Earth Sci., 89, 522–532, 2000.
1329 Niessen, F., Hong, J. K., Hegewald, A., Matthiessen, J., Stein, R., Kim, H., Kim, S., Jensen, L.,
1330 Jokat, W., Nam, S.-I., and Kang, S.-H.: Repeated Pleistocene glaciation of the East
1331 Siberian Continental Margin, Nat. Geosci., 6, 842-846, 2013.
1332 Niewohner, C., Hensen, C., Kasten, S., Zabel, M., and Schulz, H. D.: Deep sulfate reduction
1333 completely mediated by anaerobic methane oxidation in sediments of the upwelling area
1334 off Namibia, Geochim. Cosmochim. Ac., 62, 455–464, 1998.
1335 Nöthen, K. and Kasten, S.: Reconstructing changes in seep activity by means of pore water and
1336 solid phase Sr/Ca and Mg/Ca ratios in pockmark sediments of the Northern Congo Fan,
1337 Mar. Geol., 287, 1-13, 2011.
1338 O'Regan, M., Williams, C. J., Frey, K. E., Jakobsson, M.: A synthesis of the long-term
1339 paleoclimatic evolution of the Arctic. Oceanography 24(3), 66–80, 2011

1340 O'Regan, M., Preto, P., Stranne, C., Jakobsson, M., and Koshurnikov, A.: Surface heat flow
1341 measurements from the East Siberian continental slope and southern Lomonosov Ridge,
1342 Arctic Ocean, Geochem. Geophy. Geosy., 17, 1-15, 2016.
1343 Ostanin, I., Anka, Z., di Primio, R. and Bernal, A.: Hydrocarbon plumbing systems above the
1344 Snøhvit gas field: structural control and implications for thermogenic methane leakage in
1345 the Hammerfest Basin, SW Barents Sea. Marine and Petroleum Geology, 43, 127-146,
1346 2013.
1347 Party, S. S.: Integrated Ocean Drilling Program Expedition 303 Preliminary Report North
1348 Atlantic Climate Ice sheet–ocean atmosphere interactions on millennial timescales during
1349 the late Neogene-Quaternary using a paleointensity-assisted chronology for the North
1350 Atlantic, 1-51, 2005.
1351 Paull, C. K., Ussler, W. III, and Dillon, W. P.: Is the extent of glaciation limited by marine gas-
1352 hydrates?, Geophys. Res. Lett., 18 432–434, 1991.
1353 Paull, C. K., Matsumoto, R., Wallace, P. J., and Shipboard Scientific Party: Proceedings of the
1354 IODP, Initial Reports. Volume 164: College Station, TX, USA, 1996.
1355 Paull, C. K, Lorenson, T. D., Borowski, W. S., Ussler, III W., Olsen, K., and Rodriguez, N. M.:
1356 Isotopic composition of CH_4, CO_2 species, and sedimentary organic matter within
1357 samples from the Blake Ridge: gas source implications, In: Paull C. K., Matsumoto, R,
1358 Wallace, P. J., and Dillon, W. P., (Eds) Proceedings of the ODP, Sci. Res., Vol. 164 67–
1359 78, (ODP), 2000.
1360 Pecher, I. A., Kukowski, N., Huebscher, C., Greinert, J., and Bialas, J.: The link between bottom-
1361 simulating reflections and methane flux into the gas hydrate stability zone - new evidence
1362 from Lima Basin, Peru Margin, Earth Planet. Sc. Lett., 185, 343-354, 2001.

1363 Peterson, B. J., Holmes, R. M., McClelland, J. W., Vorosmarty, C. J., Lammers, R. B.,
1364 Shiklomanov, A. I., Shiklomanov, I. A., and Rahmstorf, S.: Increasing river discharge to
1365 the Arctic Ocean, Science, 298, 2171–2173, 2002.
1366 Petersen, C. J., Bünz, S., Hustoft, S., Mienert, J., and Klaeschen, D.: High-resolution P-Cable 3D
1367 seismic imaging of gas chimney structures in gas hydrated sediments of an Arctic
1368 sediment drift, Mar. Petrol. Geol., 1–14, 2010.
1369 Phrampus, B. J., Hornbach, M. J., Ruppel, C. D., and Hart P. E.: Widespread gas hydrate
1370 instability on the upper US Beaufort margin, J. Geophys. Res-Sol. Ea., 119, 8594–8609,
1371 2014
1372 Piñero, E., Marquardt, M., Hensen, C., Haeckel, M., and Wallmann K.: Estimation of the global
1373 inventory of methane hydrates in marine sediments using transfer functions,
1374 Biogeosciences 10, 959–975, 2013.
1375 Pohlman, J. W., Riedel, M., Waite, W., Rose, K., and Lapham, L.: Application of Rhizon
1376 samplers to obtain high-resolution pore-fluid records during geo-chemical investigations
1377 of gas hydrate systems, Fire in the Ice: Methane Hydrate Newsletter, US Department of
1378 Energy/National Energy Technology Laboratory, Fall, 2008.
1379 Posewang, J. and Mienert, J.: High-resolution seismic studies of gas hydrates west of Svalbard,
1380 Geo-Mar. Lett., 19, 150–156, 1999.
1381 Prell, W. L., Niitsuma, N., and Shipboard Scientific Party: Proceedings of the Ocean Drilling
1382 Program, Initial Reports, 117: College Station, TX (Ocean Drilling Program), 1998.
1383 Rachor, E.: The expedition ARK-XI/1 of RV" Polarstern" in 1995: [ARK XI/1, Bremerhaven-
1384 Tromsø-, 07.07. 1995-20.09. 1995]. Berichte zur Polarforschung (Reports on Polar
1385 Research), 226, 1995.

1386 Reagan, M. T. and Moridis, G. J.: Dynamic response of oceanic hydrate deposits to ocean
1387 temperature change, J. Geophys. Res., 113, 1-21, 2008.
1388 Reagan, M. T. and Moridis, G. J.: Large-scale simulation of methane hydrate dissociation along
1389 the West Spitsbergen margin, Geophys. Res. Lett., 36, 1-5, 2009.
1390 Redfield, A. C.: The biological control of chemical factors in the environment, Am. Sci., 46,
1391 221-230, 1958.
1392 Regnier, P., Dale, A. W., Arndt, S., LaRowe, D. E., Mogollón, J., and Van Cappellen, P.:
1393 Quantitative analysis of anaerobic oxidation of methane (AOM) in marine sediments: a
1394 modeling perspective, Earth-Sci. Rev., 106, 105-130, 2011.
1395 Reeburgh, W. S.: Methane consumption in Cariaco Trench waters and sediments, Earth Planet
1396 Sci. Lett., 28, 337–344, 1976.
1397 Riedel, M., Collett, T.S., Malone, M.J., and the Expedition 311 Scientists Proceedings of the
1398 Integrated Ocean Drilling Program, Volume 311, 2006.
1399 Riedinger, N., Kasten, S., Gröger, J., Franke, C. and Pfeifer, K.: Active and buried authigenic
1400 barite fronts in sediments from the Eastern Cape Basin, Earth Planet. Sc. Lett., 241, 876-
1401 887, 2006.
1402 Riedinger, N., Formolo, M. J., Lyons, T. W., Henkel, S., Beck, A., and Kasten, S.: An inorganic
1403 geochemical argument for coupled anaerobic oxidation of methane and iron reduction in
1404 marine sediments, Geobiology, 12, 172-181, 2014.
1405 Rudels, B., Muench, R. D., Gunn, J., Schauer, U., and Friedrich, H. J.: Evolution of the Arctic
1406 Ocean boundary current north of the Siberian shelves, Journal of Marine Systems, 25, 1,
1407 77-99, 2000.

Biogeosciences Discuss., doi:10.5194/bg-2016-308, 2016
Manuscript under review for journal Biogeosciences
Published: 9 August 2016

1408 Ryan, W. B. F., Carbotte, S. M., Coplan, J. O., O'Hara, S., Melkonian, A., Arko, R., Weissel, R.
1409 A., Ferrini, V., Goodwillie, A., Nitsche, F., Bonczkowski, J., and Zemsky, R.: Global
1410 Multi-Resolution Topography synthesis, Geochem. Geophys. Geosyst., 10, 1-9, 2009.
1411 Sander, B. C. and Kalff, J.: Factors controlling bacterial production in marine and freshwater
1412 sediments, Microb. Ecol., 26, 79-99, 1993.
1413 Sauvage, J.: Dissolved Inorganic Carbon and Alkalinity in Marine Sedimentary Interstitial
1414 Water, Master Thesis, University of Rhode Island, 2013.
1415 Schrum, H. S., Murray, R. S., and Gribsholt B.: Comparison of rhizon sampling and whole round
1416 squeezing for marine sediment porewater, Sci. Drill., 13, 47–50, 2012.
1417 Schulz, H. D.: Quantification of early diagenesis: dissolved constituents in marine pore water, In
1418 Mar. Geochem., Springer Berlin Heidelberg, 85-128, 2000.
1419 Seeberg-Elverfeldt, J., Schlüter, M., Feseker, T., and Kölling, M.: Rhizon sampling of pore
1420 waters near the sediment/water interface of aquatic systems, Limnol. Oceanogr. Methods,
1421 3, 361-371, 2005.
1422 Seifert, R. and Michaelis, W.: Organic compounds in sediments and pore waters of Sites 723 and
1423 724, In Prell, W.L., Niitsuma, N., et al., Proc. ODP, Sci. Results, 117: College Station,
1424 TX (ODP), 529–545, 1991.
1425 Serreze, M. C., Walsh, J. E., Chapin, III F. S., Osterkamp, T., Dyurgerov, M., Romanovsky, V.,
1426 Oechel, W. C., Morison, J., Zhang T., and Barry, R. B.: Observational evidence of recent
1427 change in the northern high-latitude environment, Climatic Change, 46, 159–207, 2000.
1428 Semiletov, I., Makshtas, O. A., Akasofu, S.I., and Andreas, E. L.: Atmospheric CO2 balance: the
1429 role of Arctic sea ice, Geophys. Res. Lett., 31, 1-4, 2004.

Biogeosciences Discuss., doi:10.5194/bg-2016-308, 2016
Manuscript under review for journal Biogeosciences
Published: 9 August 2016

1430 Shakhova, N, Semiletov, I, Salyuk, A, Yusupov, V, Kosmach, D, and Gustafsson, Ö.: Extensive
1431 Methane venting to the atmosphere from sediments of the East Siberian arctic shelf,
1432 Science, 327, 1246–1250, 2010a.
1433 Shakhova, N., Semiletov, I., Leifer, I., Rekant, P., Salyuk, A., and Kosmach, D.: Geochemical
1434 and geophysical evidence of methane release from the inner East Siberian Shelf, J.
1435 Geophys. Res., 115, 1-14, 2010b.
1436 Sher, A. V., Kuzmina, S. A., Kuznetsova, T. V., and Sulerzhitsky, L. D.: New insights into the
1437 Weichselian environment and climate of the East Siberian Arctic, derived from fossil
1438 insects, plants, and mammals, Quaternary Sci. Rev., 24, 533 – 569, 2005.
1439 Shipboard Scientific Party: Leg 201 summary, In D'Hondt, S.L., Jørgensen, B.B., Miller, D.J., et
1440 al., Proc. ODP, Init. Repts., 201: College Station TX (Ocean Drilling Program), 1–81,
1441 2003.
1442 Smith, J. P. and Coffin, R. B.: Methane Flux and Authigenic Carbonate in Shallow Sediments
1443 Overlying Methane Hydrate Bearing Strata in Alaminos Canyon, Gulf of Mexico,
1444 Energies, 7, 6118-6141, 2014.
1445 Snyder, G. T., Hiruta, A., Matsumoto, R., Dickens, G. R., Tomaru, H., Takeuchi, R.,
1446 Komatsubara, J., Ishida, Y., and Yu, H.: Porewater profiles and authigenic mineralization
1447 in shallow marine sediments above the methane-charged system on Umitaka Spur, Japan
1448 Sea. Deep-Sea Research II 54, 1216–1239, 2007.
1449 Soloviev, V. A.: Gas-hydrate-prone areas of the ocean and gas-hydrate accumulations, Journal of
1450 the Conference Abstracts, 6, 158, 2002.

1451 Spielhagen, R. F., Werner, K., Sorensen, S. A., Zamelczyk, K., Kandiano, E., Budeus, G.,
1452 Husum, K., Marchitto, T. M., and Hald, M.: Enhanced modern heat transfer to the Arctic
1453 by warm Atlantic water, Science 331, 450-453, 2011.
1454 Stein, R., Boucsein, B., and Meyer, H.: Anoxia and high primary production in the Paleogene
1455 central Arctic Ocean: First detailed records from Lomonosov Ridge, Geophys. Res. Lett.,
1456 33, 1-6, 2006.
1457 Stein, R.: Arctic Ocean sediments: processes, proxies, and paleoenvironment, Developments in
1458 Mar. Geol., 2. Elsevier, Amsterdam. 592 pp., 2008.
1459 Stranne, C., O'Regan, M., Dickens, G. R., Crill, P., Miller, C., Preto, P., and Jakobsson, M.:
1460 Dynamic simulations of potential methane release from East Siberian continental slope
1461 sediments, Geochem. Geophy. Geosy., 17, 872-886, 2016.
1462 Stroeve, J. C., Serreze, M. C., Holland, M. M., Kay, J. E., Malanik, J., and Barrett, A. P.: The
1463 Arctic's rapidly shrinking sea ice cover: a research synthesis, Climatic Change, 110,
1464 1005-1027, 2012.
1465 Suess, E., von Huene, R., and Shipboard Scientific Party: Proceedings of the Ocean Drilling
1466 Program, Initial Reports, 112: College Station, TX (Ocean Drilling Program), 1988.
1467 Takahashi, T. Broecker, V. S., and Langer, S.: Redfield ratio based on chemical data from
1468 isopycnal surfaces, J. Geophys. Res-Oceans, 90, 6907-6924, 1985.
1469 Takahashi, K., Ravelo, A.C., Alvarez Zarikian, C.A., and the Expedition 323 Scientists
1470 Proceedings of the Integrated Ocean Drilling Program, Volume 323, 2011.
1471 Tamaki, K., Pisciotto, K., Allan, J., and Shipboard Scientific Party: Proceedings of the Ocean
1472 Drilling Program, Initial Reports, Vol. 127, 1990.

Biogeosciences Discuss., doi:10.5194/bg-2016-308, 2016
Manuscript under review for journal Biogeosciences
Published: 9 August 2016

1473 Thatcher, K. E., Westbrook, G. K., Sarkar, S., and Minshull, T. A.: Methane release from
1474 warming-induced hydrate dissociation in the West Svalbard continental margin: Timing,
1475 rates, and geological controls, J. Geophys. Res-Sol. Ea., 118, 22–38, 2013.
1476 Timokhov L. A.: Regional characteristics of the Laptev and the East Siberian seas: climate,
1477 topography, ice phases, thermohaline regime, and circulation, In: Russian-German
1478 cooperation in the Siberian Shelf seas: geo-system Laptev Sea, H. Kassens, H. W.
1479 Hubberten, S. Priamikov and R. Stein, editors. Berichte zur Polarforschung, 144, 15-31,
1480 1994.
1481 Torres, M. E., Kastner, M., Wortmann, U. G., Colwell, F., and Kim, J.: Estimates of methane
1482 production rates based on δ13C of the residual DIC in pore fluids from the Cascadia
1483 margin, EOS, 8(52), Fall Meet. Suppl., Abstract GC14A04, 2007.
1484 Torres, M. E. and Kastner M.: Data report: Clues about carbon cycling in methane-bearing
1485 sediments using stable isotopes of the dissolved inorganic carbon, IODP Expedition 311,
1486 Proceedings of the IODP, 311, 2009.
1487 Treude, T., Krause, S., Maltby, J., Dale, A.W., Coffin, R. and Hamdan, L.J.: Sulfate reduction
1488 and methane oxidation activity below the sulfate-methane transition zone in Alaskan
1489 Beaufort Sea continental margin sediments: Implications for deep sulfur cycling.
1490 Geochimica et Cosmochimica Acta, 144, 217-237, 2014
1491 Troup, B. N., Bricker, O. P., and Bray, J. T.: Oxidation effect on the analysis of iron in the
1492 interstitial water of recent anoxic sediments, Nature 249, 237-239, 1974.
1493 Ussler, W. and Paull, C.K.: Rates of anaerobic oxidation of methane and authigenic carbonate
1494 mineralization in methane-rich deep-sea sediments inferred from models and
1495 geochemical profiles. Earth and Planetary Science Letters, 266(3), 271-287, 2008.

Biogeosciences Discuss., doi:10.5194/bg-2016-308, 2016
Manuscript under review for journal Biogeosciences
Published: 9 August 2016

1496 Vanneste, M., Guidard, S., and Mienert, J.: Bottom-simulating reflections and geothermal
1497 gradients across the western Svalbard margin, Terra Nova, 17, 510–516, 2005.
1498 Wallmann, K., Pinero, E., Burwicz, E., Haeckel, M., Hensen, C., Dale, A. W., and Ruepke, L.:
1499 The global inventory of methane hydrate in marine sediments: A theoretical approach,
1500 Energies, 5, 2449–2498, 2012.
1501 Wang, G., Spivack, A. J., and D'Hondt, S.: Gibbs energies of reaction and microbial mutualism
1502 in anaerobic deep subseafloor sediments of ODP Site 1226, Geochim. Cosmochim. Ac.,
1503 74, 3938-3947, 2010.
1504 Weaver, J. S. and Stewart, J. M.: In-situ hydrates under the Beaufort Sea Shelf, In: M.H. French
1505 (Editor), Proceedings of the Fourth Canadian Permafrost Conference 1981, Roger J. E.
1506 Brown Memorial Volume, Nat. Res. Council Can., Ottawa, Ont., 312-319, 1982.
1507 Wefer, G., Berger, W. H., Richter, C., and Shipboard Scientific Party: Proceedings of the Ocean
1508 Drilling Program, Initial Reports, 175: College Station, TX (Ocean Drilling Program),
1509 1998.
1510 Woodgate R. A., Aaagard, K., Muench, R. D., Gunn, J., Björk, G., Rudels, B., Roach, A. T., and
1511 Schauer, U.: The Arctic Ocean boundary current along the Eurasian slope and the
1512 adjacent Lomonosov Ridge: Water mass properties, transports and transformation from
1513 moored instruments, Deep Sea Research, 48, 1757-1792, 2001.
1514 Yamamoto, K. and Dallimore, S.: Aurora-JOGMEC-NRCan Mallik 2006–2008 Gas Hydrate
1515 Research Project progress. In: Fire in the Ice, NETL Methane Hydrate Newsletter,
1516 Summer 2008, 1–5, 2008.

Biogeosciences Discuss., doi:10.5194/bg-2016-308, 2016
Manuscript under review for journal Biogeosciences
Published: 9 August 2016

1517 Ye, H., Yang, T., Zhu, G., Jiang, S., and Wu, L.: Pore water geochemistry in shallow sediments
1518 from the northeastern continental slope of the South China Sea, Mar. Petrol. Geol., 75,
1519 68-82, 2016.
1520 Yoshinaga, M. Y., Holler, T., Goldhammer, T., Wegener, G., Pohlman, J. W., Brunner, B.,
1521 Kuypers, M. M., Hinrichs, K. U. and Elvert, M.: Carbon isotope equilibration during
1522 sulphate-limited anaerobic oxidation of methane. Nature Geoscience, 7(3), 190-194,
1523 2014.
1524

Biogeosciences Discuss., doi:10.5194/bg-2016-308, 2016
Manuscript under review for journal Biogeosciences
Published: 9 August 2016

1525 **Figures**

1526 **Figure 1.**

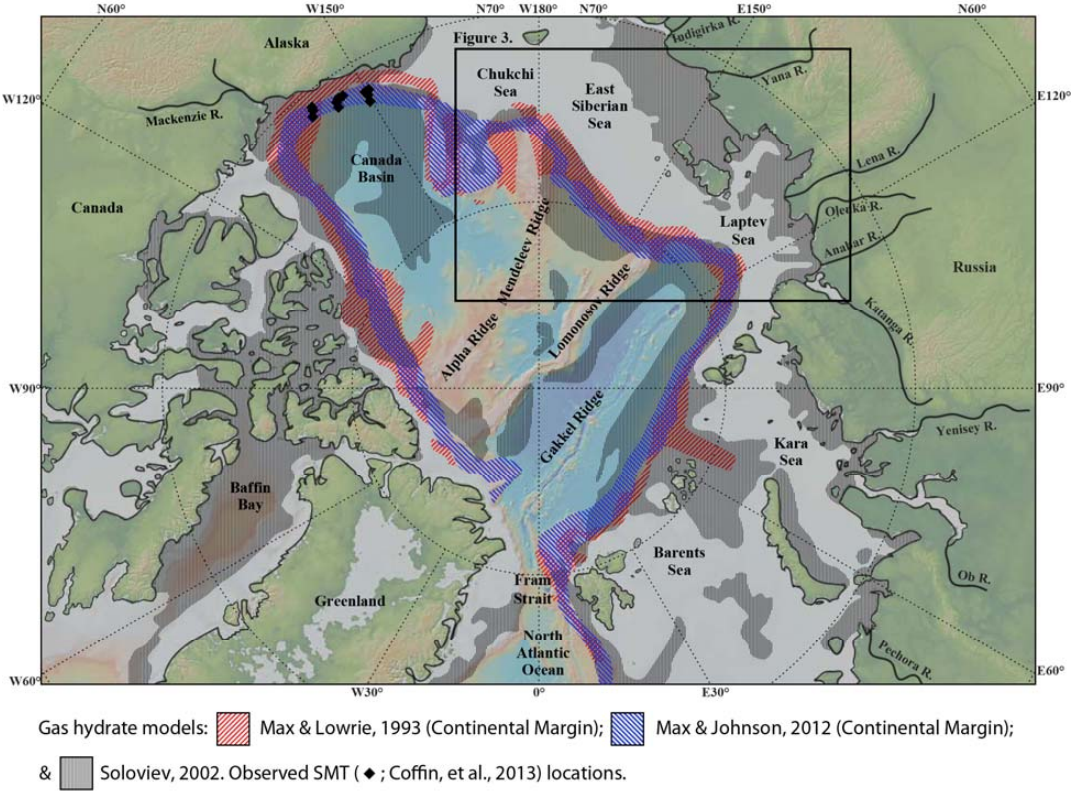

1527

Biogeosciences Discuss., doi:10.5194/bg-2016-308, 2016
Manuscript under review for journal Biogeosciences
Published: 9 August 2016

1528 **Figure 2.**

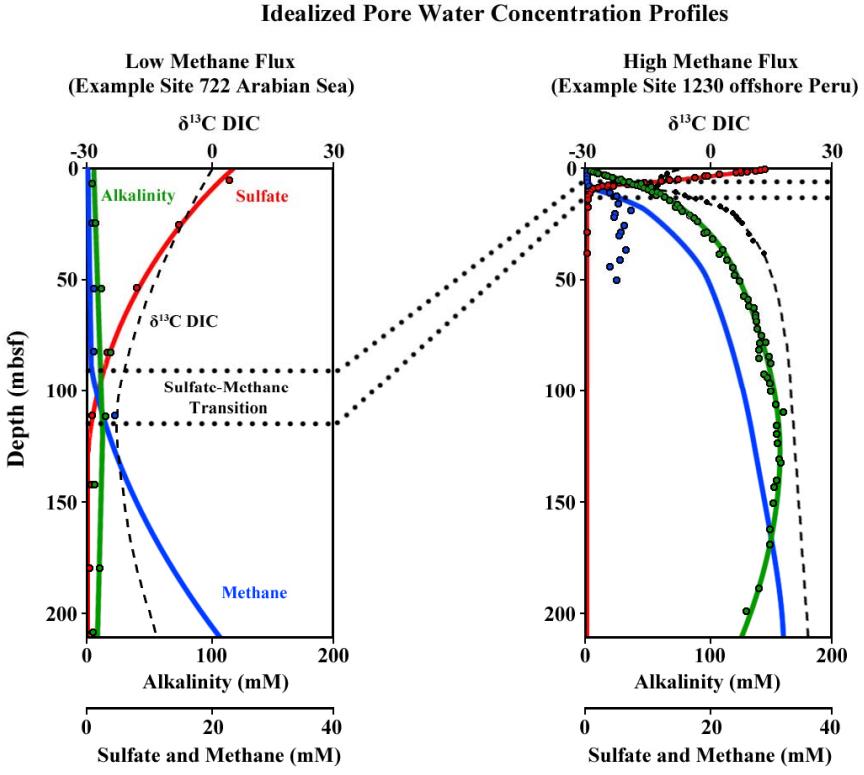

1529
1530
1531
1532
1533
1534
1535
1536
1537
1538
1539
1540
1541

Biogeosciences Discuss., doi:10.5194/bg-2016-308, 2016
Manuscript under review for journal Biogeosciences
Published: 9 August 2016

1542 **Figure 3.**

1543

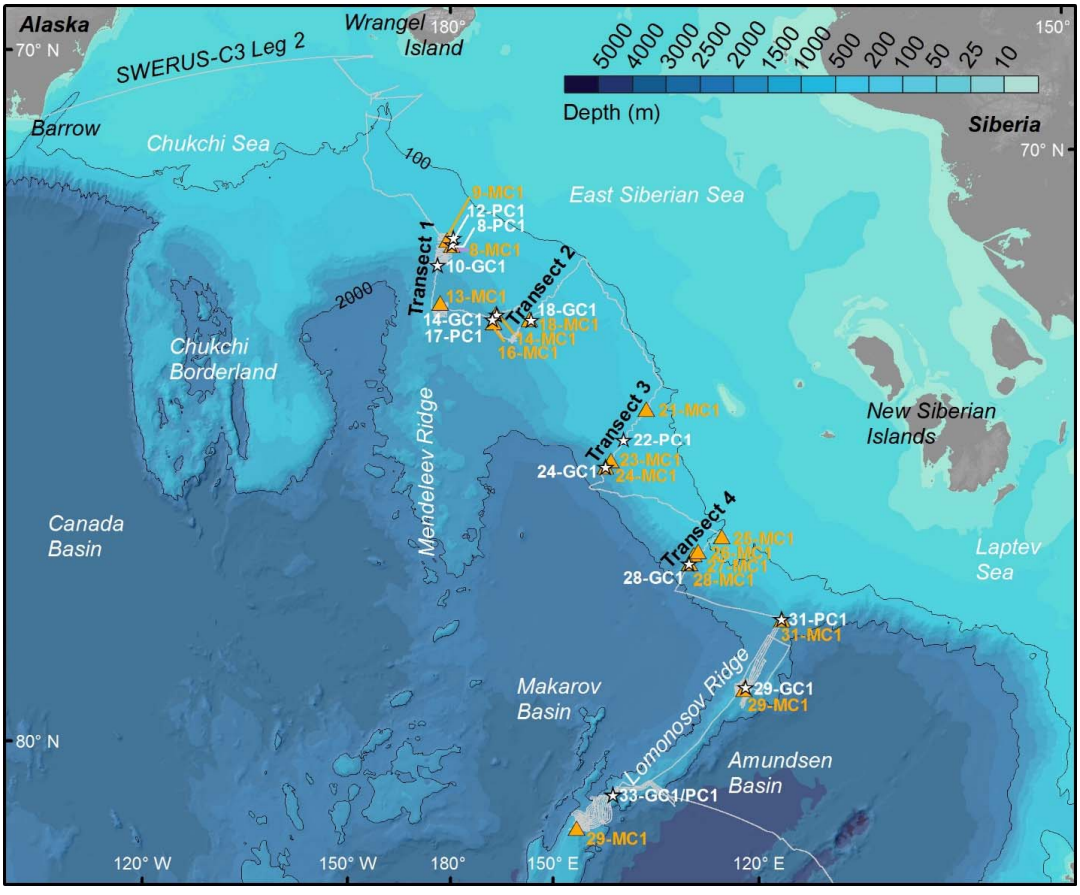

1544

1545

1546

1547

1548

1549

1550

1551

1552

1553

1554

Biogeosciences Discuss., doi:10.5194/bg-2016-308, 2016
Manuscript under review for journal Biogeosciences
Published: 9 August 2016

1555 **Figure 4.**

(a.)

(b.)

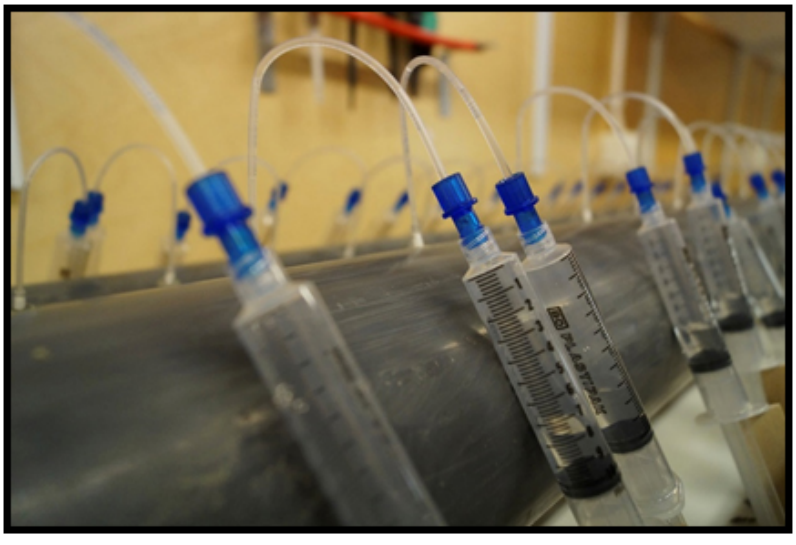

1556
1557
1558
1559
1560
1561

Biogeosciences Discuss., doi:10.5194/bg-2016-308, 2016
Manuscript under review for journal Biogeosciences
Published: 9 August 2016

1562 **Figure 5.**

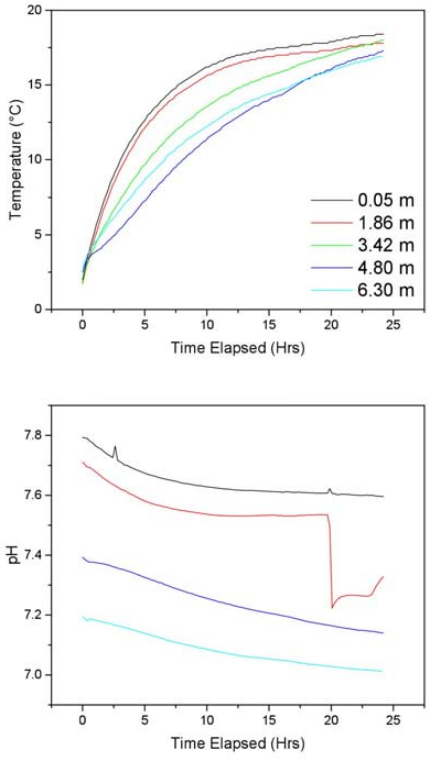

1563

Biogeosciences Discuss., doi:10.5194/bg-2016-308, 2016
Manuscript under review for journal Biogeosciences
Published: 9 August 2016

1564 **Figure 6.**

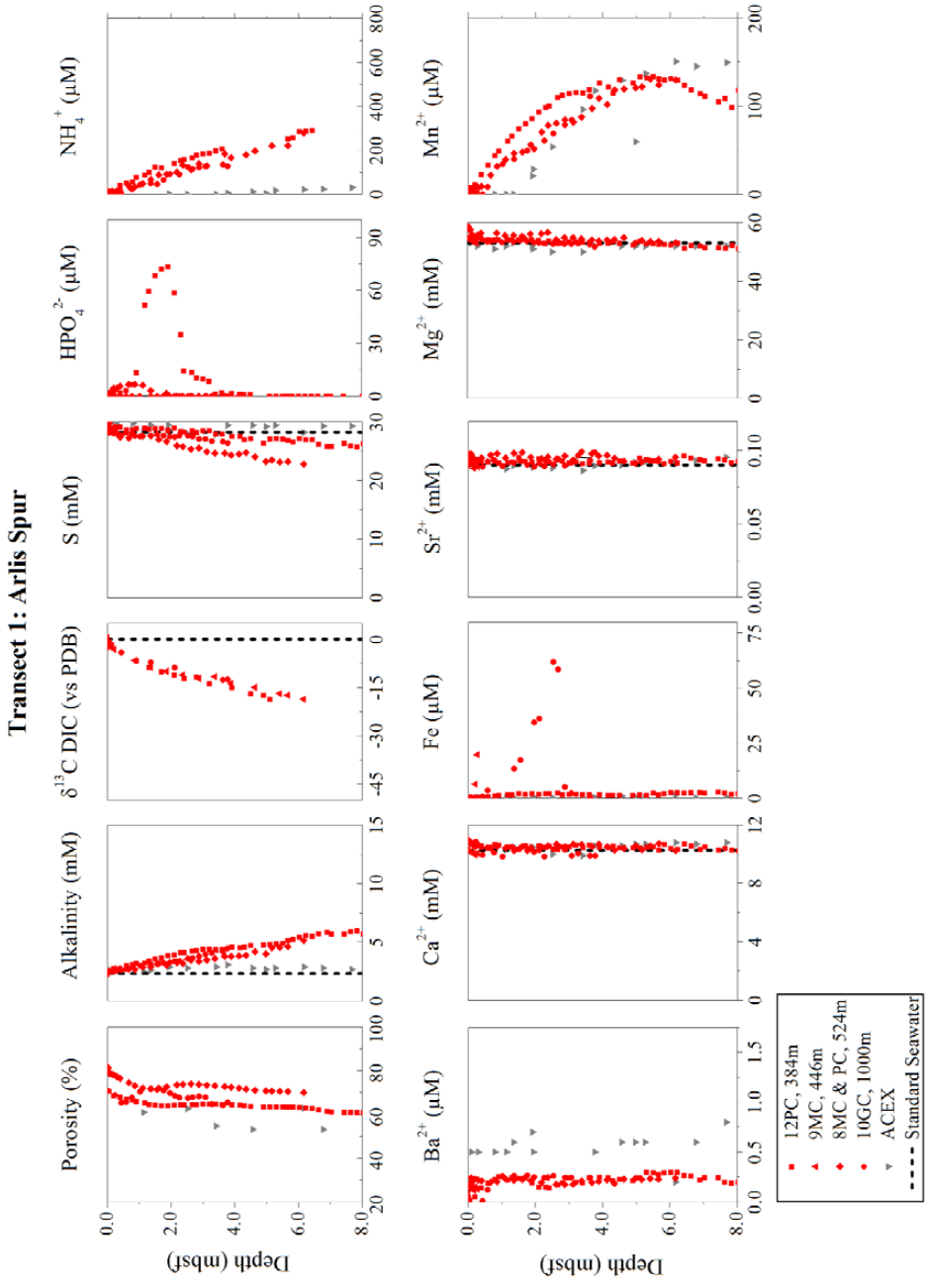

1565

1566

Biogeosciences Discuss., doi:10.5194/bg-2016-308, 2016
Manuscript under review for journal Biogeosciences
Published: 9 August 2016

1567 **Figure 7.**

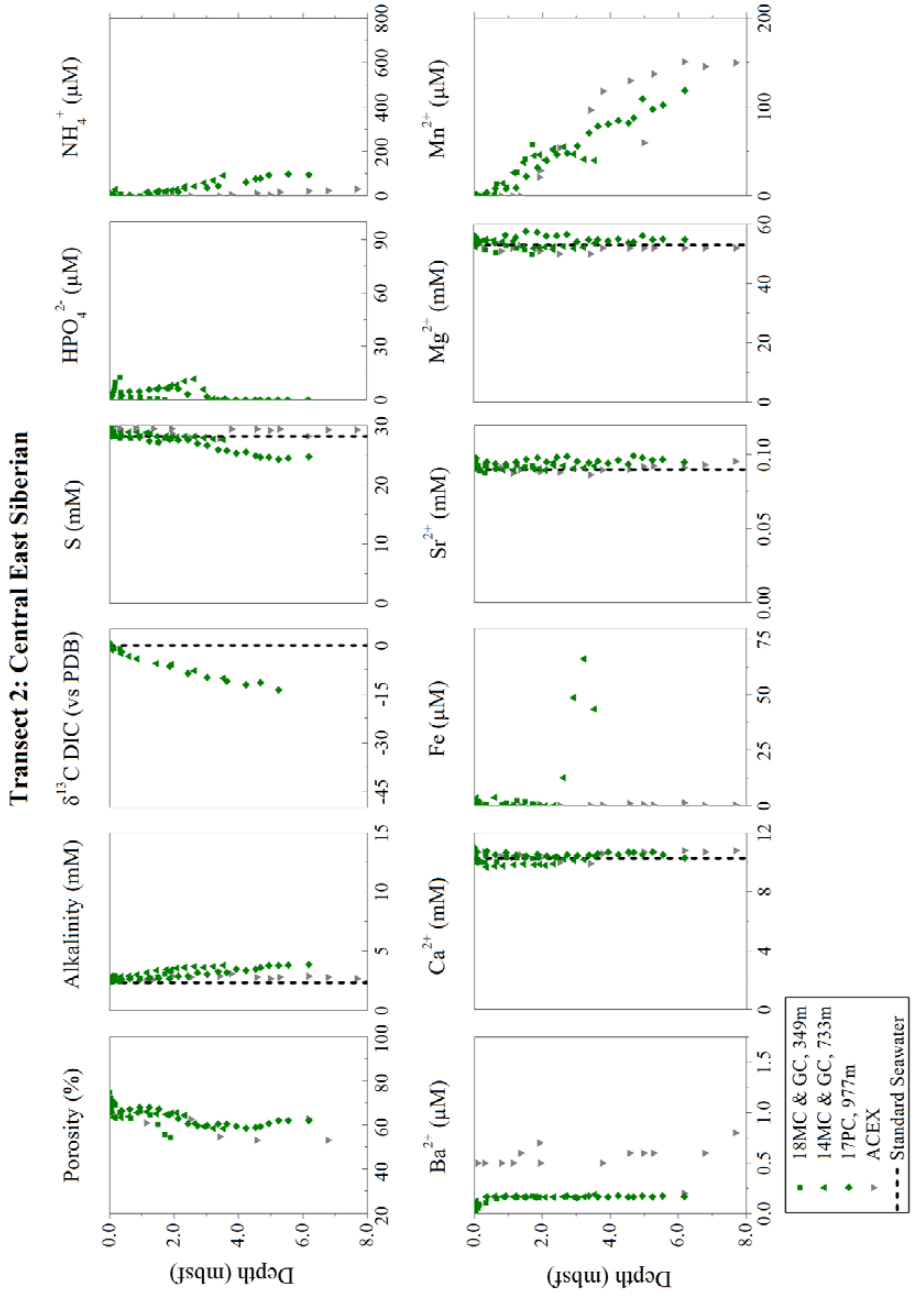

1568

1569

Biogeosciences Discuss., doi:10.5194/bg-2016-308, 2016
Manuscript under review for journal Biogeosciences
Published: 9 August 2016

1570 **Figure 8.**

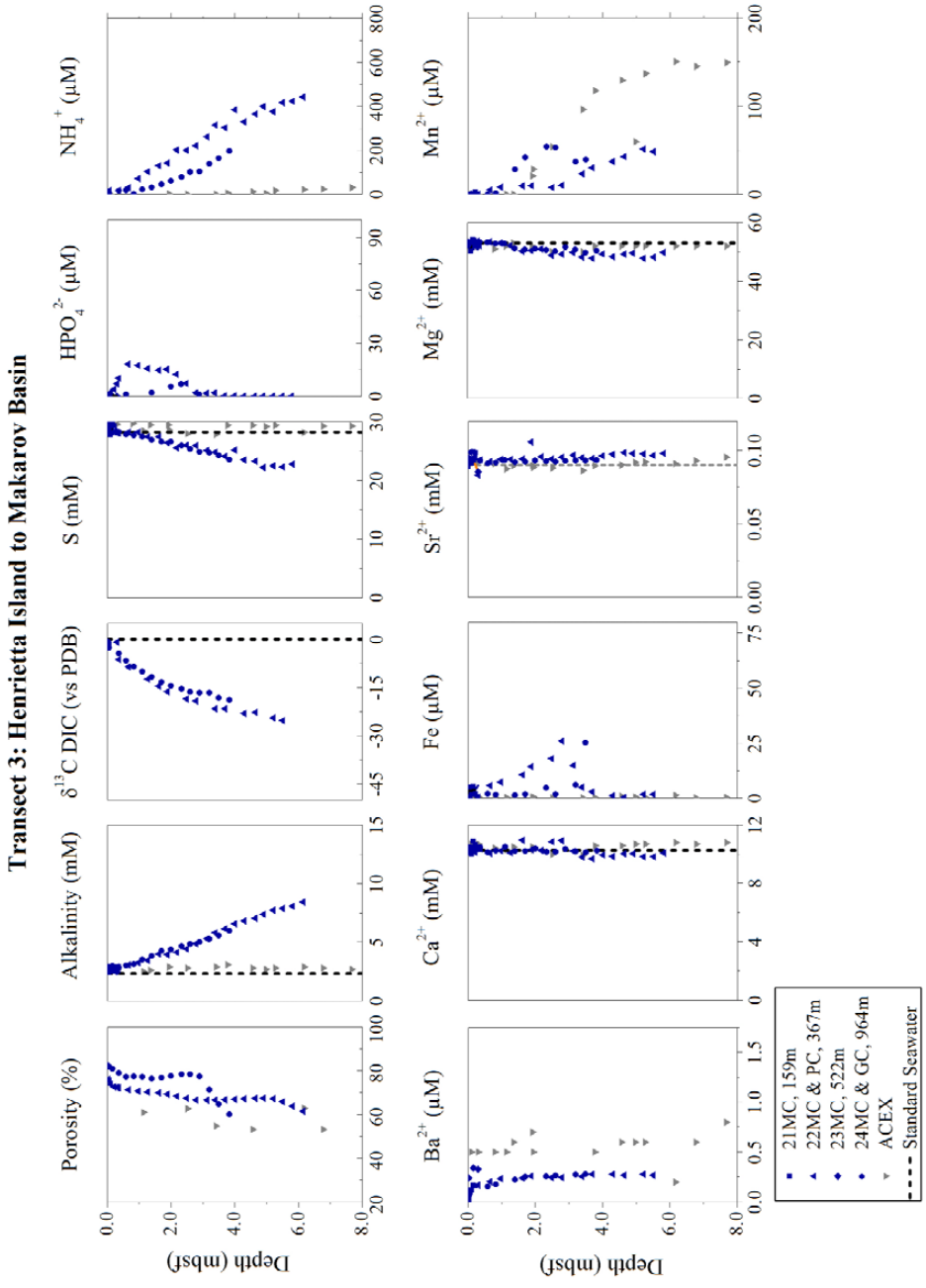

1571

1572

Biogeosciences Discuss., doi:10.5194/bg-2016-308, 2016
Manuscript under review for journal Biogeosciences
Published: 9 August 2016

1573 **Figure 9.**

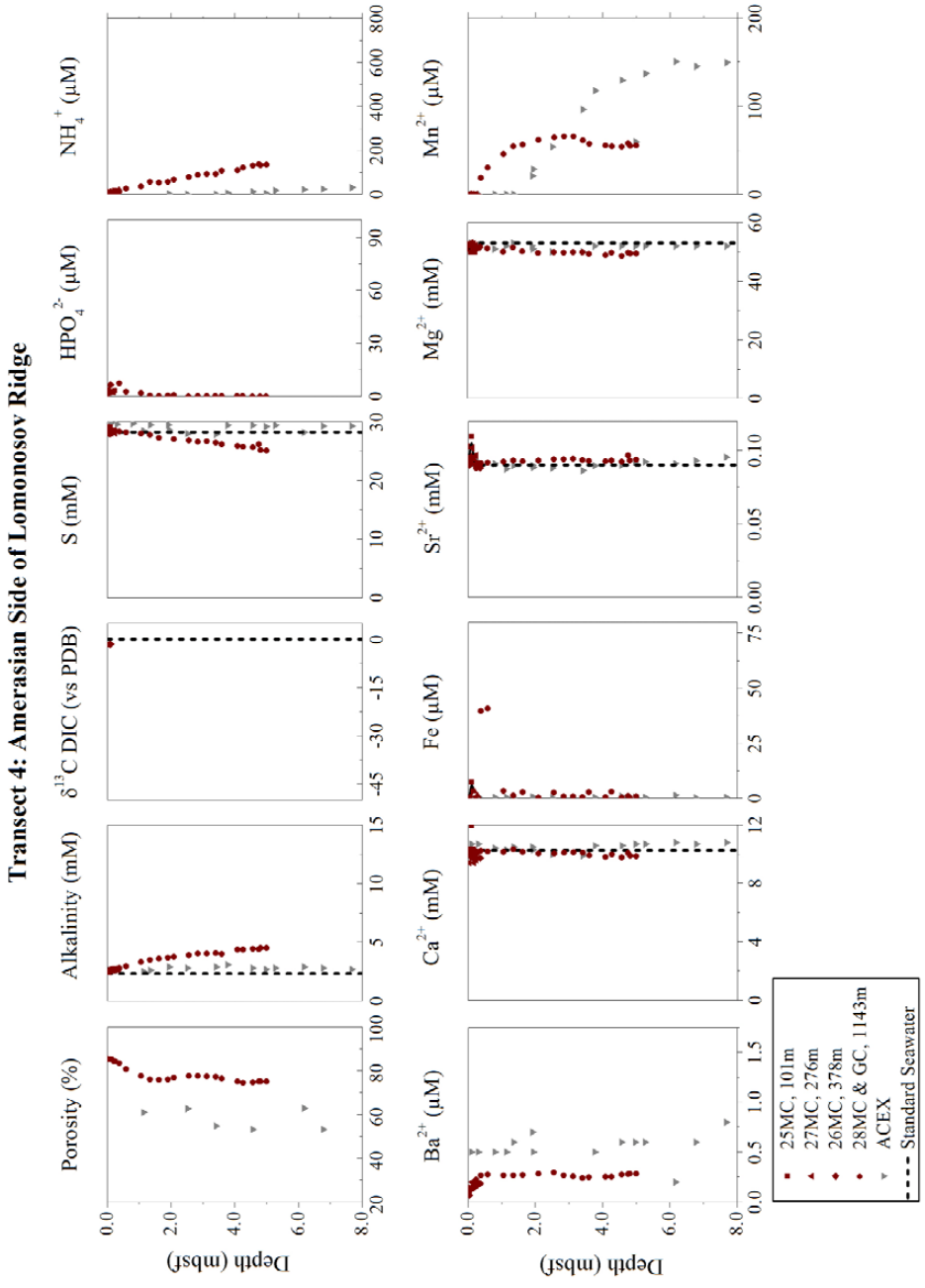

1574

1575

Biogeosciences Discuss., doi:10.5194/bg-2016-308, 2016
Manuscript under review for journal Biogeosciences
Published: 9 August 2016

1576 **Figure 10.**

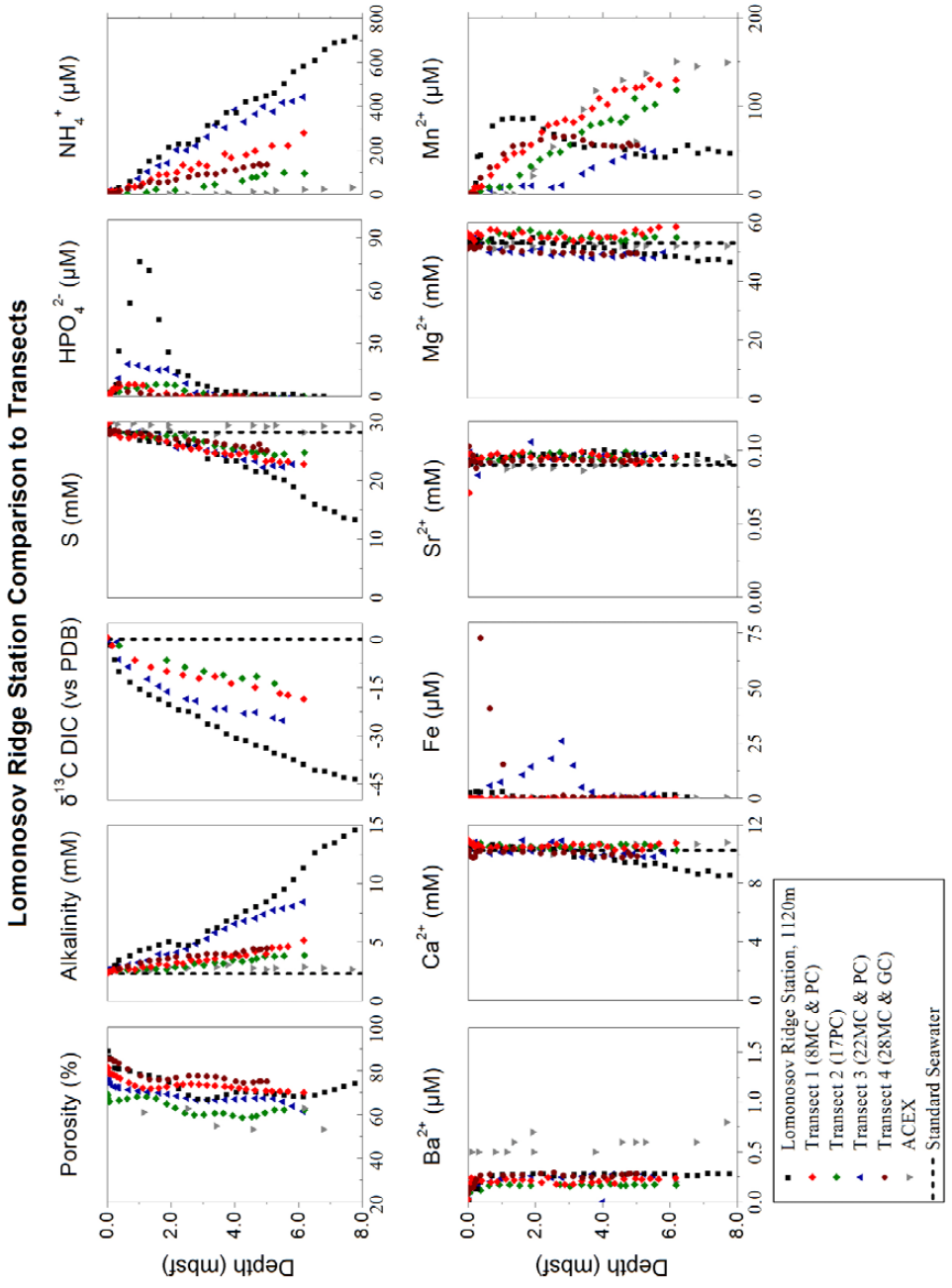

1577

1578

Biogeosciences Discuss., doi:10.5194/bg-2016-308, 2016
Manuscript under review for journal Biogeosciences
Published: 9 August 2016

1579 **Figure 11.**

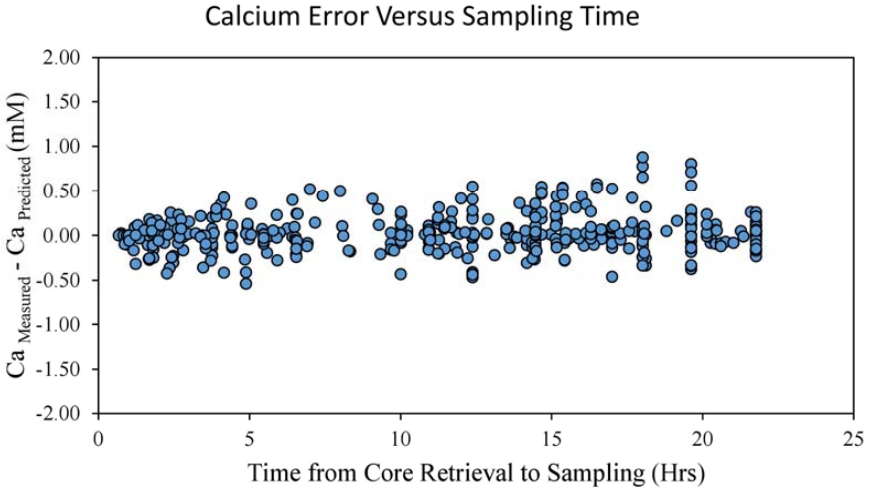

1580
1581
1582
1583
1584
1585
1586
1587
1588
1589
1590
1591
1592
1593
1594
1595
1596
1597

Biogeosciences Discuss., doi:10.5194/bg-2016-308, 2016
Manuscript under review for journal Biogeosciences
Published: 9 August 2016

1598 **Figure 12.**

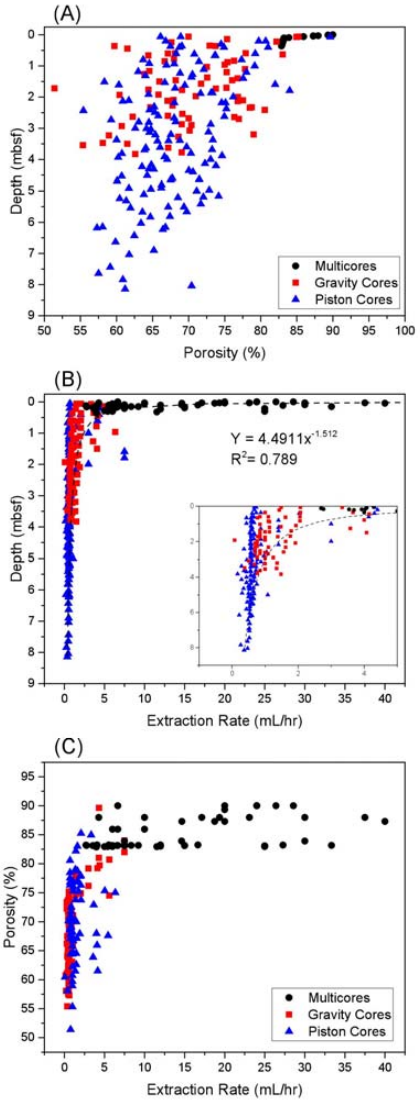

1599

1600

1601

1602

1603

1604

Biogeosciences Discuss., doi:10.5194/bg-2016-308, 2016
Manuscript under review for journal Biogeosciences
Published: 9 August 2016

1605 **Figure 13.**

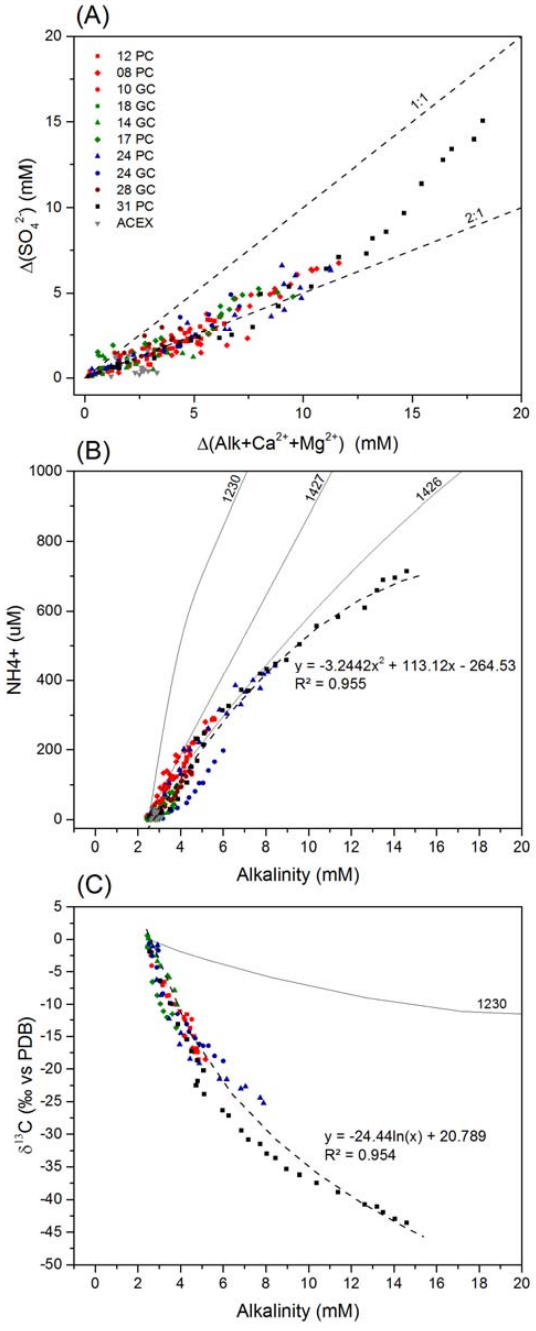

1606

Biogeosciences Discuss., doi:10.5194/bg-2016-308, 2016
Manuscript under review for journal Biogeosciences
Published: 9 August 2016

1607 **Figure 14.**

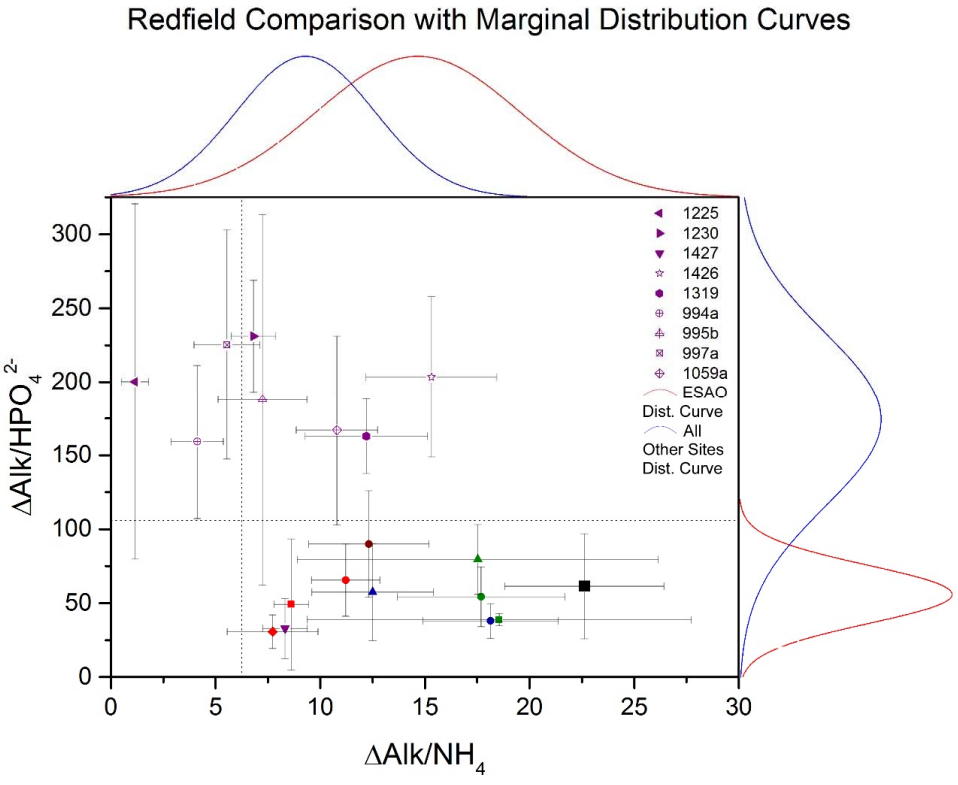

1608

Biogeosciences Discuss., doi:10.5194/bg-2016-308, 2016
Manuscript under review for journal Biogeosciences
Published: 9 August 2016

1609 **Figure 15.**

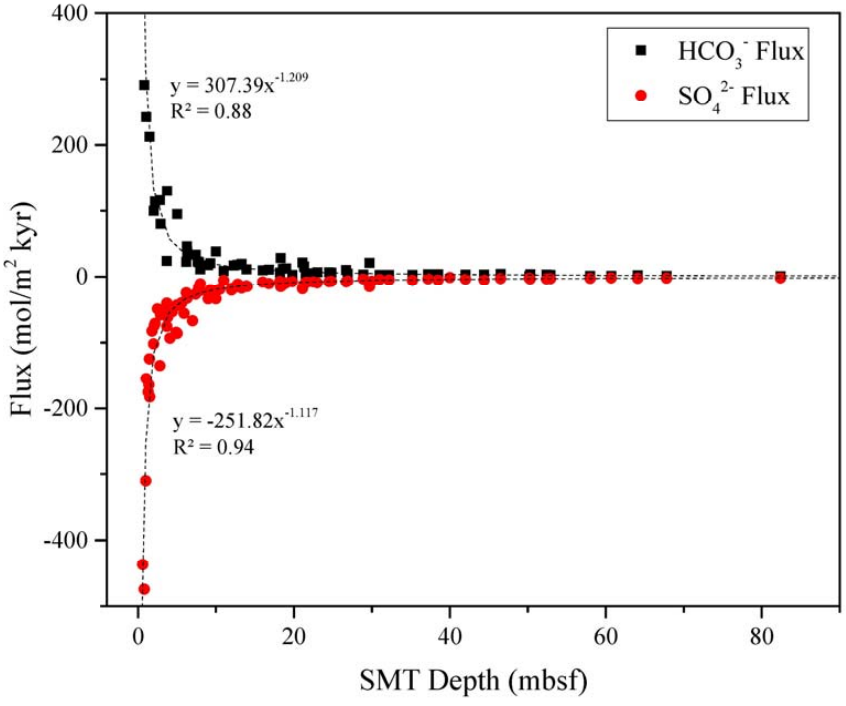

1610

1611

1612

1613

1614

1615

1616

1617

1618

1619

1620

1621

Biogeosciences Discuss., doi:10.5194/bg-2016-308, 2016
Manuscript under review for journal Biogeosciences
Published: 9 August 2016

1622 **Figure 16.**

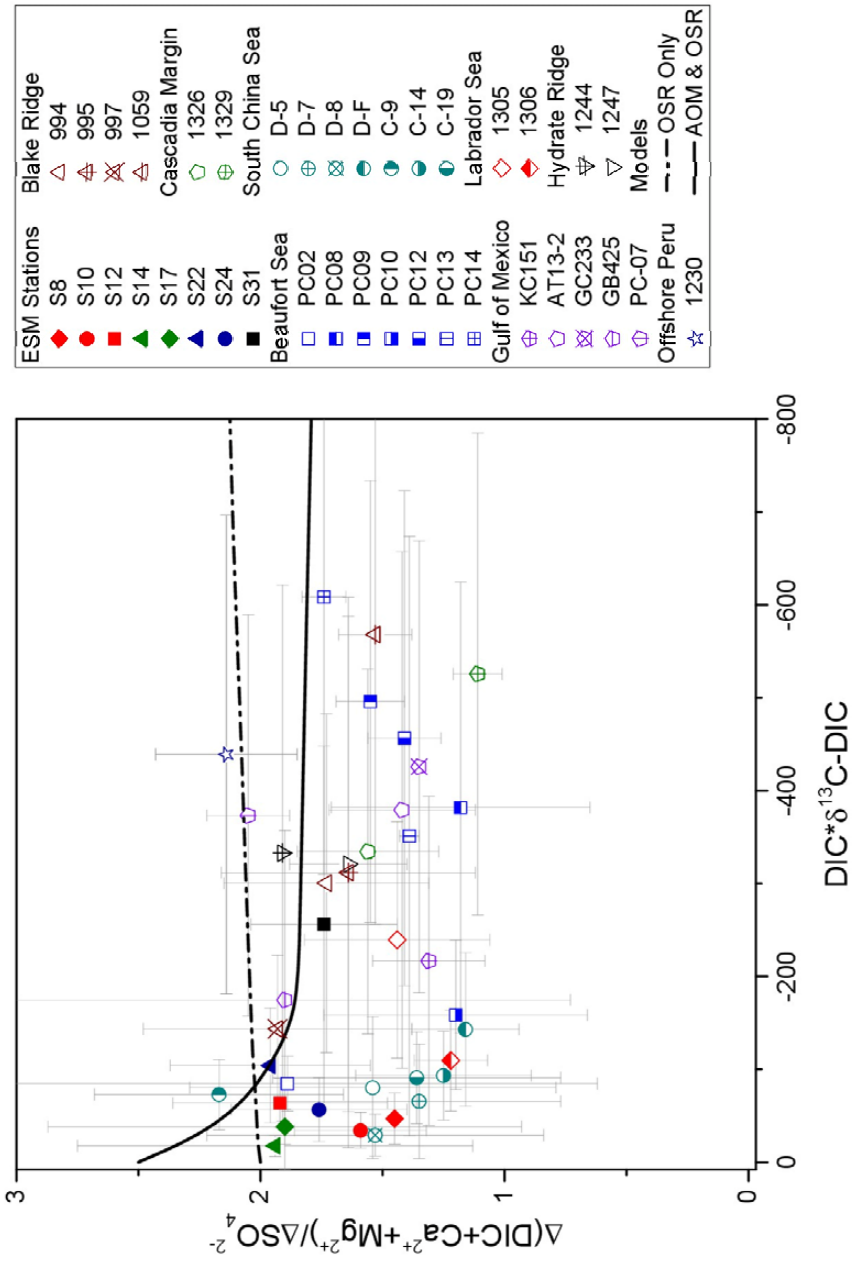

1623

Biogeosciences Discuss., doi:10.5194/bg-2016-308, 2016
Manuscript under review for journal Biogeosciences
Published: 9 August 2016

Biogeosciences
Discussions
Open Access
EGU

Table 1 Rhizon Efficacy

Station	Location		Water Depth	Core Type	Core Length	Total Time from Coring to Sampling		Rhizon Extraction Time	
	Latitude	Longitude	(m)		(m)	Average (hrs)	Range (hrs)	Average (hrs)	Range (hrs)
8	75° 09' 11.4912" N	179° 52' 23.0952" E	524	MC	0.16	0.92	(0.57 - 1.15)	0.47	(0.08 - 1.21)
9	75° 03' 24.2166" N	179° 49' 13.497" W	446	MC	0.29	1.13	(0.87 - 1.26)	0.91	(0.19 - 1.47)
13	76° 11' 10.7772" N	179° 16' 42.102" W	1118	MC	0.17	1.40	(1.20 - 1.68)	0.40	(0.20 - 0.68)
14	76° 21' 10.3926" N	176° 27' 39.9954" E	733	MC	0.20	2.51	(0.83 - 4.42)	1.76	(0.08 - 3.67)
16	76° 30' 43.2540" N	176° 37' 55.1670" E	1023	MC	0.21	2.81	(1.87 - 3.70)	1.44	(0.51 - 2.33)
18	76° 24' 32.8680" N	173° 52' 44.9178" E	349	MC	0.33	2.11	(1.32 - 2.68)	1.21	(0.42 - 1.78)
21	77° 34' 56.4918" N	163° 17' 36.7326" E	159	MC	0.24	4.02	(3.45 - 4.37)	0.73	(0.17 - 1.08)
22	78° 13' 25.9572" N	164° 25' 36.3612" E	367	MC	0.32	0.73	(0.68 - 0.75)	0.38	(0.33 - 0.41)
23	78° 39' 51.7206" N	165° 01' 57.8352" E	522	MC	0.32	1.48	(0.67 - 1.93)	1.24	(0.35 - 1.85)
24	78° 48' 00.1080" N	165° 22' 55.8552" E	982	MC	0.32	1.79	(0.85 - 2.18)	1.34	(0.52 - 1.67)
25	79° 13' 34.6362" N	152° 40' 32.2284" E	101	MC	0.25	0.97	(0.83 - 1.17)	0.63	(0.51 - 0.83)
26	79° 44' 31.6782" N	154° 23' 20.3244" E	378	MC	0.37	1.83	(0.80 - 2.80)	1.53	(0.50 - 2.51)
27	79° 39' 52.6824" N	154° 07' 34.5324" E	276	MC	0.26	1.65	(1.35 - 2.18)	1.30	(1.01 - 1.83)
28	79° 55' 10.3584" N	154° 21' 12.7578" E	1145	MC	0.27	1.53	(0.85 - 2.27)	1.10	(0.42 - 1.83)
29	81° 20' 33.9750" N	141° 46' 31.6668" E	899	MC	0.23	1.55	(1.05 - 2.05)	1.17	(0.67 - 1.67)
31	79° 55' 13.4070" N	143° 09' 53.0994" E	1157	MC	0.39	2.38	(1.80 - 3.38)	2.08	(1.50 - 3.08)
32	85° 08' 28.2582" N	151° 35' 24.5220" E	837	MC	0.33	4.38	(2.38 - 5.05)	3.33	(1.33 - 4.01)
Multicore Average and Range					0.27	1.95	(0.57 - 5.05)	1.24	(0.08 - 4.01)
8	75° 08' 06.3342" N	179° 51' 05.9004" E	515	PC	6.42	18.56	(4.81 - 20.85)	15.22	(1.78 - 17.5)
10	75° 30' 12.6462" N	179° 05' 59.265" W	1000	GC	3.99	11.01	(3.38 - 12.38)	10.31	(1.83 - 11.83)
12	75° 00' 57.3114" N	179° 45' 09.9900" E	384	PC	8.43	21.44	(20.27 - 21.77)	17.95	(16.42 - 19.15)
14	76° 22' 04.9146" N	176° 25' 56.9670" E	737	GC	2.75	14.58	(6.55 - 17.11)	9.00	(5.22 - 10.01)
17	76° 27' 52.6248" N	176° 43' 25.7628" E	977	PC	6.37	19.62	(18.12 - 19.62)	16.58	(15.08 - 16.58)
18	76° 24' 41.7240" N	173° 47' 17.6454" E	351	GC	1.95	7.72	(3.02 - 14.37)	6.40	(1.73 - 12.92)
22	78° 13' 22.5336" N	164° 27' 42.6306" E	364	PC	6.45	19.79	(13.5 - 25.17)	17.71	(11.42 - 23.08)
24	78° 47' 48.9186" N	165° 21' 59.5080" E	964	GC	4.05	12.25	(10.94 - 14.19)	5.89	(4.83 - 7.42)
28	79° 55' 28.0302" N	154° 23' 44.7180" E	1143	GC	5.23	12.78	(3.33 - 14.33)	6.98	(5.58 - 16.63)
29	81° 17' 57.6816" N	141° 46' 57.1794" E	824	GC	4.66	17.43	(9.25 - 18.02)	13.38	(4.72 - 14.12)
31	79° 54' 53.4270" N	143° 14' 00.4488" E	1120	PC	8.07	11.95	(3.90 - 18.07)	9.25	(1.33 - 15.50)
33	84° 16' 29.5422" N	148° 44' 07.1484" E	886	GC	3.59	12.20	(9.57 - 19.07)	8.55	(5.92 - 15.42)
33	84° 16' 55.3368" N	148° 38' 48.3102" E	888	PC	6.24	11.06	(7.55 - 17.88)	9.48	(5.82 - 16.25)
Gravity/Piston Core Average and Range					5.25	14.65	(3.02 - 25.17)	11.28	(1.33 - 23.08)

Biogeosciences Discuss., doi:10.5194/bg-2016-308, 2016
Manuscript under review for journal Biogeosciences
Published: 9 August 2016

Table 2 Rhizon Flow Rates

Station	Flow Rate (mL/hr)			Flow Rate Decrease per meter
	Average	Min	Max	(mL/hr/m)
8	25.28	8.33	37.50	243.06
9	11.36	5.16	26.82	59.21
13	23.68	14.63	33.33	70.36
14	8.31	0.55	24.00	130.30
16	8.31	0.55	24.00	79.37
18	10.77	3.93	26.40	70.23
21	13.00	2.77	40.00	201.71
22	26.82	25.00	30.00	18.52
23	13.52	5.41	28.57	77.22
24	9.51	6.00	19.35	49.46
25	16.24	12.00	20.00	36.36
26	8.85	4.00	20.00	49.23
27	8.09	5.45	10.00	21.65
28	11.80	5.45	24.00	74.18
29	10.36	6.00	16.50	58.33
31	5.16	3.24	6.67	10.07
32	5.21	3.75	11.25	23.44
Multicore Average	12.72	6.60	23.43	74.86
8	1.13	0.29	5.61	0.84
10	1.35	0.38	5.45	1.33
12	0.53	0.17	0.67	0.04
14	1.19	1.00	1.92	0.14
17	0.61	0.36	0.73	0.02
18	2.76	0.08	6.35	2.83
22	0.59	0.22	0.88	0.11
24	1.71	1.25	2.07	0.20
28	1.74	0.70	3.00	0.70
29	0.80	0.64	2.12	0.35
31	2.03	0.65	7.50	0.19
33	1.26	0.65	1.69	0.14
33	1.11	0.62	1.69	0.13
Gravity/Piston Core Average	1.29	0.54	3.05	0.54

1625

1626

1627

Biogeosciences Discuss., doi:10.5194/bg-2016-308, 2016
Manuscript under review for journal Biogeosciences
Published: 9 August 2016

Table 3 QA/QC Results

Analysis	Sample Type	Number	Result
Alkalinity	Spiked	15	PE = 1.53%
Alkalinity	Duplicate	8	PD = 1.30%
δ^{13}C-DIC	Seawater Standard	2	0.23‰ and 0.32‰
δ^{13}C-DIC	Blind Field Duplicate	4	PD = 22.98%
δ^{13}C-DIC	Field Blank	1	No Result
δ^{13}C-DIC	Duplicate	10	PD = 14.70%
Metals	Spiked	51	RSD = 2.55% (Ba), 2.17% (Ca), 1.53% (Fe), 0.77% (Mg), 1.73% (Mn), 1.88% (S), and 1.42% (Sr)
Metals	Blind Field Duplicate	11	PD = 2.56% (Ba), 3.77% (Ca), 5.81% (Fe), 2.68% (Mg), 3.07% (Mn), 0.71% (S), and 3.79% (Sr)
Metals	Field Blank	2	BDL
Phosphate	VKI Standard	2	PE = 1.28% and 2.69%
Ammonia	VKI Standard	2	PE = 2.40% and 6.25%

Notes: PE = Percent Error
PD = Percent Difference
RSD = Relative Standard Deviation
BDL = Below Detection Limit

Biogeosciences Discuss., doi:10.5194/bg-2016-308, 2016
Manuscript under review for journal Biogeosciences
Published: 9 August 2016

Table 4 - Reported and Calculated Fluxes

Ocean	Location	Water Depth (m)	SMT Depth (mbsf)	SO_4^{2-} Flux (mol/m^2kyr)	Alkalinity Flux (mol/m^2kyr)	$\delta^{13}C$ at SMT (‰)
Arctic	Beaufort Sea - Cape Halkett[a,b]	280	1.06	-154.8	242.6	-21.5
Arctic	Beaufort Sea - Cape Halkett[a,b]	342	1.47	-124.7	212.3	-20.2
Arctic	Beaufort Sea - Cape Halkett[a,b]	1005	3.73	-44.2	130.3	-18.2
Arctic	Beaufort Sea - Cape Halkett[a,b]	1458	6.29	-27.4	46.3	-19.7
Arctic	East Siberian Slope	349	61	-1.8	1.7	--
Arctic	East Siberian Slope	367	25	-6.9	6.3	--
Arctic	East Siberian Slope	384	64	-2.4	2.3	--
Arctic	East Siberian Slope	524	35	-5.6	2.8	--
Arctic	East Siberian Slope	733	58	-2.1	1.5	--
Arctic	East Siberian Slope	977	58	-2.1	1.6	--
Arctic	East Siberian Slope	964	23	-9.2	6.8	--
Arctic	East Siberian Slope	1000	52	-3.3	3.3	--
Arctic	East Siberian Slope	1143	44	-5.1	3.5	--
Arctic	East Siberian Slope	1120	14	-13.9	11.3	--
Atlantic	New Jersey Continental Slope[q,i]	912	28.9	-3.3	3.6‡	--
Atlantic	Blake Ridge[q,p]	1293	50.3	-3.4	3.8‡	--
Atlantic	Blake Ridge[q,p]	1798	26.9	-6.6	4.9‡	--
Atlantic	Blake Ridge[q,x]	2567	42.0	-3.8	3.5‡	--
Atlantic	Blake Ridge[q,x]	2641	24.5	-7.6	6.9‡	--
Atlantic	Blake Ridge[q,x]	2777	21.7	-8.3	5.4‡	--
Atlantic	Blake Ridge[q,x]	2770	22.5	-7.8	4.7‡	--
Atlantic	Blake Ridge[q,x]	2798	21.5	-8.7	4.4‡	--
Atlantic	Blake Ridge[q,p]	2985	9.3	-20.0	20.4‡	--
Atlantic	Blake Ridge[q,p]	3481	12.3	-17.1	17.0‡	--
Atlantic	Blake Ridge[q,p]	4040	16.8	-10.5	10.8‡	--
Atlantic	Gulf of Mexico - Keathley Canyon[w]	1300	9	-33‡	17‡	-49.6
Atlantic	Gulf of Mexico - Atwater Valley[w]	1300	0.1	-2901	--	--
Atlantic	Gulf of Mexico - Atwater Valley[w]	1300	0.1	-2901	--	--
Atlantic	Gulf of Mexico - Atwater Valley[w]	1300	0.6	-437	--	--
Atlantic	Gulf of Mexico - Atwater Valley[w]	1300	7	-67	--	-46.3
Atlantic	Amazon Fan[q,v,y]	3191	37.2	-3.2	4.1‡	-39.8
Atlantic	Amazon Fan[q,v,y]	3474	6.2	-24.6	22.7‡	-47.5
Atlantic	Amazon Fan[q,v,y]	3704	3.7	-40.3	24.3‡	-49.6
Atlantic	Western Africa[q,z]	426	12.8	-12.5	18.2‡	--
Atlantic	Western Africa[q,z]	738	52.9	-3.1	2.9‡	--
Atlantic	Western Africa[q,z]	1280	21.3	-12.0	15.6‡	-19.8
Atlantic	Western Africa[q,z]	1402	18.3	-14.9	28.3‡	--

Biogeosciences Discuss., doi:10.5194/bg-2016-308, 2016
Manuscript under review for journal Biogeosciences
Published: 9 August 2016

Atlantic	Western Africa[q,z]	1713	38.5	-5.1	4.1‡	--
Atlantic	Western Africa[q,z]	2179	26.7	-7.8	10.4‡	--
Atlantic	Western Africa[q,z]	2382	21.1	-18.1	21.8‡	--
Atlantic	Western Africa[q,z]	2995	29.7	-14.9	20.9‡	--
Atlantic	Argentine Basin[l]	1228	10.5	-19.1	--	--
Atlantic	Argentine Basin[l]	1492	12	-20.2	--	--
Atlantic	Argentine Basin[l]	1568	4.9	-84.6	--	--
Atlantic	Argentine Basin[l]	1789	5.9	-55.6	--	--
Atlantic	Argentine Basin[l]	3247	10	-21.8	--	--
Atlantic	Argentine Basin[l]	3167	14	-14.7	--	--
Atlantic	Argentine Basin[l]	3542	3.7	-75.4	--	--
Atlantic	Argentine Basin[l]	3551	5.6	-39.9	--	--
Atlantic	Argentine Basin[l]	3551	4.1	-93.3	--	--
Atlantic	Argentine Basin[l]	3623	5	-43.1	--	--
Atlantic	Argentine Basin[l]	4280	5.1	-43.5	--	--
Atlantic	Argentine Basin[l]	4799	12	-17.9	--	--
Indian	Oman[q,1]	591	50.2	-2.2	1.1‡	--
Indian	Oman[q,1]	804	46.5	-2.8	4.4‡	--
Indian	Oman[q,1]	1423	82.4	-1.8	0.8‡	--
Pacific	Bering Sea[p,2]	1008	6.3	-32.8	37.8	-25.1
Pacific	Cascadia[q,u,2]	959	9.0	-23.6	--	-23.8
Pacific	Cascadia[q,u,2]	1322	7.9	-21.3	--	-30.8
Pacific	Cascadia[q,u,2]	1828	2.5	-49.0	--	-33.9
Pacific	Cascadia - Hydrate Ridge[o]	834	8	-10.9	11.3	-19.6
Pacific	Cascadia - Hydrate Ridge[o]	850	7.65	-22.3	23.2	-30.2
Pacific	Cascadia - Hydrate Ridge[o]	871	7.4	-26.6	33.4	-24.9
Pacific	Cascadia - Hydrate Ridge[g]	896	7.8	-16	22	-22.5
Pacific	Umitaka Spur[h]	900	2.2	-71	114	--
Pacific	Umitaka Spur[h]	947	2.9	-58	80	--
Pacific	Umitaka Spur[h]	1034	2.0	-102	100	--
Pacific	Japan Sea[s,4]	901	10	-33.6	38.4‡	--
Pacific	California Margin[q,5]	955	13.3	-17.3	19.6‡	--
Pacific	California Margin[q,5]	1564	19.0	-9.3	12.8‡	--
Pacific	California Margin[q,5]	1926	31.0	-4.3	3.1‡	--
Pacific	Nankai Trough[q,6]	1741	32.2	-4.9	3‡	--
Pacific	Nankai Trough[s,6]	2997	11.0	-5.6	8.7‡	--
Pacific	Nankai Trough[q,6]	3020	18.2	-7.0	6.4‡	--
Pacific	Santa Barbara[k]	587	1.3	-175.2	--	--
Pacific	Soledad[k]	542	1	-310.3	--	--

Biogeosciences Discuss., doi:10.5194/bg-2016-308, 2016
Manuscript under review for journal Biogeosciences
Published: 9 August 2016

Pacific	Pescadero[k]	408	1.4	-164.3	--	--
Pacific	Magdalena[k]	600	1.5	-182.5	--	--
Pacific	Alfonso[k]	713	0.8	-474.5	--	--
Pacific	Costa Rica Margin[q,7]	3306	16.0	-8.1	9.6‡	--
Pacific	Costa Rica Margin[q,7]	4177	19.8	-7.5	3.1‡	--
Pacific	Costa Rica Margin[q,7]	4311	18.6	-12.3	12.4‡	--
Pacific	Peru Margin[s,8]	161	30	-6.9	--	--
Pacific	Peru Margin[t,9]	427	40	-1.2	--	-25.4
Pacific	Peru Margin[t,9]	5086	9	-25.0	--	-13.2
Pacific	Chilean Coast[c]	586	5.55	-22.9	--	--
Pacific	Chilean Coast[c]	723	0.33	-362.0	--	--
Pacific	Chilean Coast[c]	980	2.92	-45.3	--	--
Pacific	Chilean Coast[c]	768	10.11	-13.3	--	--
Pacific	New Zealand - Porangahau Ridge[f]	1900-2150	12.8	-11.4	--	-31.4
Pacific	New Zealand - Porangahau Ridge[f]	1900-2150	4.4	-53.3	--	-31.6
Pacific	New Zealand - Porangahau Ridge[f]	1900-2150	3.6	-50.5	--	-31.4
Pacific	New Zealand - Porangahau Ridge[f]	1900-2150	2.1	-74.2	--	-33.4
Pacific	New Zealand - Porangahau Ridge[f]	1900-2150	3.8	-61.5	--	-35.0
Pacific	New Zealand - Porangahau Ridge[f]	1900-2150	1.8	-82.6	--	-48.8
Pacific	New Zealand - Hikurangi[b,d]	350	39.5	5‡	7.3‡	--
Pacific	New Zealand - Hikurangi[b,d]	332	12.9	19.3‡	13.6‡	--
Pacific	New Zealand - Hikurangi[b,d]	98	0.87	192.1‡	160.9‡	--
Pacific	New Zealand - Hikurangi[b,d]	285	3.64	65.2‡	59.6‡	--
Southern Ocean	Antarctic - Cumberland Bay[n]	237	5.03	-86	95	-25.4
Southern Ocean	Antarctic - Cumberland Bay[n]	260	0.80	-539	291	-23.5
Southern Ocean	Antarctic - Cumberland Bay[n]	275	2.80	-135	116	-15.5

1638

1639

1640

1641

1642

1643

Biogeosciences Discuss., doi:10.5194/bg-2016-308, 2016
Manuscript under review for journal Biogeosciences
Published: 9 August 2016

1644 Appendix 1.

1645 These models follow Chatterjee et al., (2011) and Malinverno and Pohlman, (2011). The first
1646 model assumes the only sulfate reduction taking place is through OSR. Carbon fractionation
1647 through OSR is set at α = 1.01 from zero at the seafloor. Sulfate is completely consumed at 10m
1648 with a constant porosity of 70%. Diffusion is calculated by Equation 1 where the diffusivity in
1649 sediment is (Iverson and Jørgensen, 1993)

$$D_S = \frac{D_O}{(1 + n(1 - \varphi))} \quad (9)$$

1650 Diffusion in seawater (D_o) for sulfate is $0.56*10^{-5}$ cm^2/s (Iverson and Jørgensen, 1993) and
1651 $0.60*10^{-5}$ cm^2/s for bicarbonate (Li and Gregory, 1974). The saturation factor (n) was assumed to
1652 be 3 for clay/silt sediments, and the sedimentation rate was set at an arbitrary 25 cm/kyr. The
1653 conceptual framework for the second model is set to include both OSR and AOM. A SMT is set
1654 at five meters below the seafloor while sulfate reduction takes place at the surface. Carbon
1655 fractionation through AOM is set at α = 1.0175. Both downward diffusing sulfate and upward
1656 methane fluxes are set at 120 mol/m^2-kyr. The $\delta^{13}C$-CH_4 of the upward diffusing methane is set
1657 at -70‰, but an additional flux of DIC set at 20‰ is added from below the SMT.
1658